The Astronomical Journal, 141:92 (17pp), 2011 March doi:10.1088/0004-6256/141/3/92


# A QUANTITATIVE ANALYSIS OF DISTANT OPEN CLUSTERS

Kenneth A. Janes and Sadia Hoq
Astronomy Department, Boston University, Boston, MA 02215, USA
*Received 2009 December 14; accepted 2010 December 17; published 2011 February 8*

## ABSTRACT

The oldest open star clusters are important for tracing the history of the Galactic disk, but many of the more distant clusters are heavily reddened and projected against the rich stellar background of the Galaxy. We have undertaken an investigation of several distant clusters (Berkeley 19, Berkeley 44, King 25, NGC 6802, NGC 6827, Berkeley 52, Berkeley 56, NGC 7142, NGC 7245, and King 9) to develop procedures for separating probable cluster members from the background field. We next created a simple quantitative approach for finding approximate cluster distances, reddenings, and ages. We first conclude that with the possible exception of King 25 they are probably all physical clusters. We also find that for these distant clusters our typical errors are about $\pm0.07$ in $E(B-V)$, $\pm0.15$ in log(age), and $\pm0.25$ in $(m-M)_\circ$. The clusters range in age from 470 Myr to 7 Gyr and range from 7.1 to 16.4 kpc from the Galactic center.

*Key words:* Hertzsprung–Russell and C–M diagrams – open clusters and associations: general – open clusters and associations: individual (Berkeley 19, Berkeley 44, King 25, NGC 6802, NGC 6827, Berkeley 52, Berkeley 56, NGC 7142, NGC 7245, King 9) – techniques: photometric

*Online-only material:* machine-readable and VO tables

## 1. INTRODUCTION

Star clusters are convenient markers of Galactic evolution. They are easy to identify and their distances, ages, and chemical compositions can be determined with considerable confidence. Dias et al. (2002) list 1537 open clusters (see also Dias et al. 2007 for updated cluster information) and Archinal & Hynes (2003) list 2017 Galactic clusters including open clusters and globular clusters. However, most of the objects tabulated as open clusters are no more than small collections of stars. Archinal & Hynes (2003) characterized a number of objects in their catalog as "asterisms," small groups of stars, probably unrelated to one another. At the locations of many other entries in the cluster catalogs, a careful examination of sky surveys reveals no sign of clustering at all.

To probe the history of the Galaxy, it would be desirable to have a large sample of both young and old clusters, particularly including clusters located in distant parts of the Galaxy. However, the old clusters, which are of the most interest for probing the history of the Galactic disk, are relatively rare. For example, Dutra & Bica (2000) list only 103 clusters of Hyades age or greater, and the WEBDA database (http://www.univie.ac.at/webda/webda.html; see Mermilliod & Paunzen 2003) has entries for 214 clusters aged 600 Myr and greater. The more distant clusters are typically projected against a rich background of Galactic field stars; even for the most massive systems, the contrast between the cluster and the field can be rather small.

Over the course of the past several years, we have observed a selection of distant clusters with the Perkins 1.83 m telescope at Lowell Observatory, in Flagstaff, AZ (operated jointly by Lowell and Boston University). All of the clusters described in this paper have been observed previously; we selected the present group because the existing information suggests that they are likely to be old clusters, useful for probing the evolution of the Galactic disk. Nevertheless, their properties are rather poorly known, partly because they are distant, highly reddened clusters in rich star fields and partly because much of the work was done many years ago. Furthermore, as Figures 1–5 show, the contrast between the cluster population of several of these clusters and the surrounding field is rather low. The challenge, then, is to extract significant information about clusters like these.

This paper describes our observations and photometric processing (Section 2) and the procedure we used to extract the best possible photometry for each cluster (Section 3). In Section 4, we develop a quantitative procedure for using these cluster data to estimate the cluster distances, reddenings, and ages. Section 5 is a discussion of the errors that affect this analysis. Section 6 consists of comments about the individual clusters, and Section 7 is a summary of our results.

Table 1 provides information about the clusters, including revised values for their positions and sizes (see Sections 3 and 4).

## 2. OBSERVATIONS

We made all of our observations using the PRISM (Perkins Re-Imaging System) camera on the Perkins telescope. The PRISM instrument converts the f/17.5 focal ratio of the telescope to f/4.45, with a $13.3 \times 13.3$ arcmin field of view and $15\,\mu$m (0.39 arcsec) pixel scale. We used a standard Lowell Observatory *BVRI* filter set, designed to be compatible with the Landolt (1992) standard stars. The seeing ranged from about 1.5 to 2.5 arcsec, FWHM.

A log of our observations is presented in Table 2. On many nights, we observed one or more of the clusters in *B*, *V*, and *I* filters as well as a selection of Landolt (1992) standard stars. (We finished our observations and photometric transformations before the publication of the Landolt (2009) update of the *UBVRI* standard system.) On other nights we have long cluster exposures only, with no standards (usually because the conditions were non-photometric). We transformed these observations using bright stars in the cluster fields as local standard stars.

We processed all images in IRAF,[1] using nightly flat-field exposures (mostly dome flats, but occasionally sky flats). We

[1] IRAF is distributed by the National Optical Astronomy Observatory, which is operated by the Association of Universities for Research in Astronomy, Inc., under cooperative agreement with the National Science Foundation.

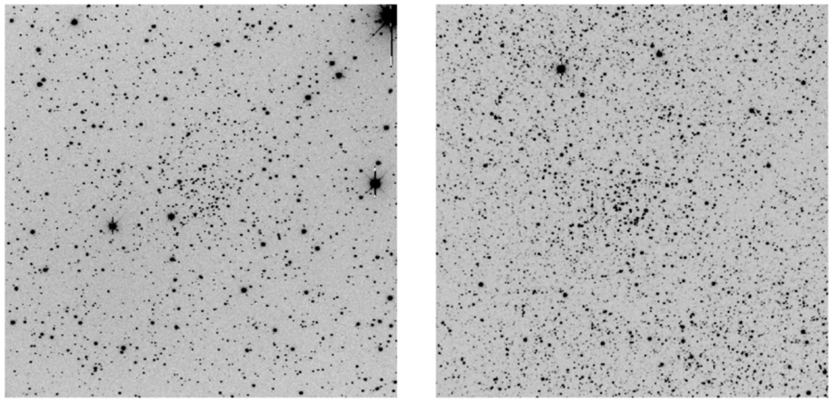

**Figure 1.** *V*-band images of Be 19 (left image) and Be 44 (right image), taken with the Perkins 1.83 m telescope. Each image covers a 13.3 arcmin field of view.

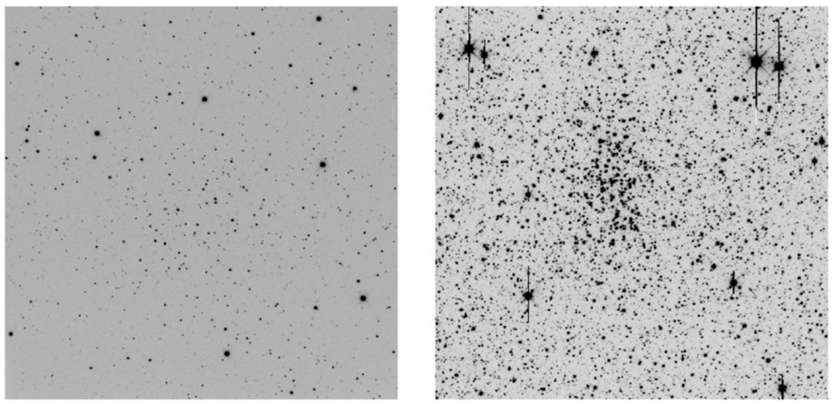

**Figure 2.** *V*-band images of King 25 (left image) and NGC 6802 (right image), taken with the Perkins 1.83 m telescope. Each image covers a 13.3 arcmin field of view.

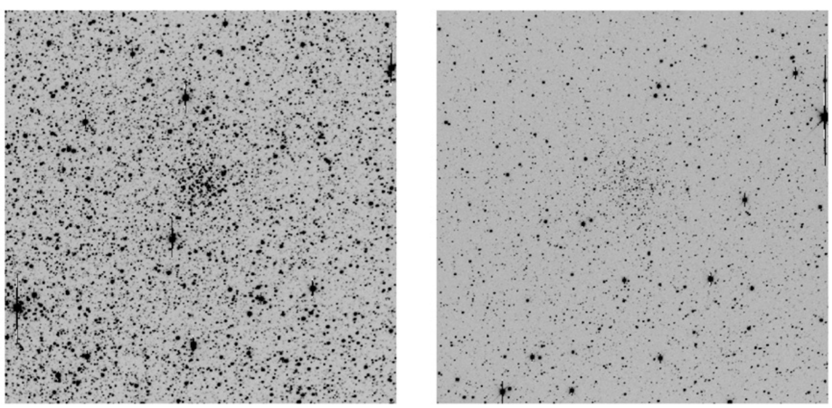

**Figure 3.** *V*-band images of NGC 6827 (left image) and Be 52 (right image), taken with the Perkins 1.83 m telescope. Each image covers a 13.3 arcmin field of view.

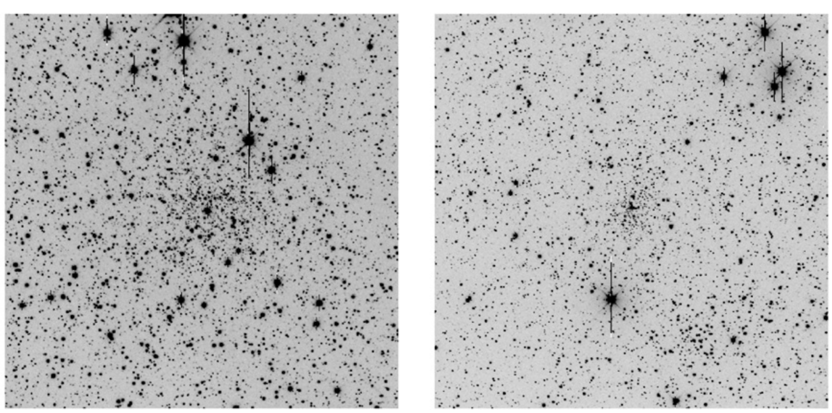

**Figure 4.** *V*-band images of Be 56 (left image) and King 9 plus NGC 7245 (right image), taken with the Perkins 1.83 m telescope. NGC 7245 is in the lower right (SW) corner of the figure. Each image covers a 13.3 arcmin field of view.

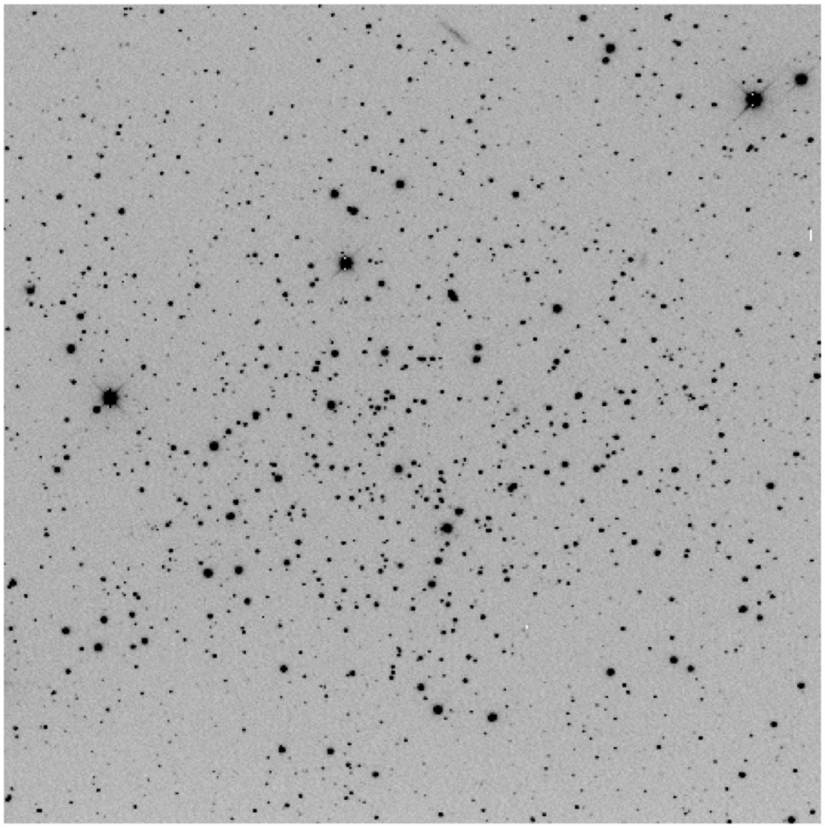

**Figure 5.** *V*-band image of NGC 7142, taken with the Perkins 1.83 m telescope. The image covers a 13.3 arcmin field of view.

**Table 1**
Summary Information for the Target Clusters

| Cluster | R.A. (h:m:s) | Decl. (°:′:″) | $\ell$ (°) | $b$ (°) | Radius (″) |
|---|---|---|---|---|---|
| Berkeley 19 | 05:24:02 | 29:33:57 | 176 | −04 | 120 |
| Berkeley 44 | 19:17:18 | 19:32:27 | 53 | +03 | 100 |
| King 25 | 19:24:36 | 13:42:06 | 49 | −01 | 170 |
| NGC 6802 | 19:30:36 | 20:15:34 | 55 | +01 | 100 |
| NGC 6827 | 19:48:53 | 21:11:52 | 58 | −02 | 60 |
| Berkeley 52 | 20:14:30 | 28:56:11 | 68 | −03 | 100 |
| Berkeley 56 | 21:17:37 | 41:49:33 | 86 | −05 | 130 |
| NGC 7142 | 21:45:10 | 65:46:18 | 105 | 10 | 240 |
| NGC 7245 | 22:15:15 | 54:19:58 | 101 | −02 | 75 |
| King 9 | 22:15:30 | 54:23:54 | 101 | −02 | 75 |

derived instrumental magnitudes for all stars in each field using the SPS program (Janes & Heasley 1993). SPS calculates a point-spread function (PSF), consisting of a Gaussian function plus a lookup table of residuals from the Gaussian, quadratically variable across the field. The PSF itself is used to create an aperture correction to scale the magnitudes to a synthetic 9.6 arcsec aperture.

For photometric transformations, we derived nightly $[V, (B-V)]$ coefficients of the form

$$v = V + \alpha_{bv}(B-V) + k_v X + C_{bv}, \tag{1a}$$

$$b = V + \alpha_b(B-V) + k_b X + C_b, \tag{1b}$$

and nightly $[V, (V-I)]$ coefficients of the form

$$v = V + \alpha_{vi}(V-I) + k_v X + C_{vi}, \tag{2a}$$

$$i = V + \alpha_i(V-I) + k_i X + C_i. \tag{2b}$$

**Table 2**
Observing Log

| Date | Stds? | Clusters |
|---|---|---|
| 2005 Mar 11 | No | Be 19 |
| 2005 Aug 31 | No | NGC 6802 |
| 2005 Sep 1 | No | NGC 6802, NGC 7245, King 9 |
| 2005 Sep 5 | No | NGC 7245, King 9 |
| 2005 Sep 23 | No | NGC 7245, King 9 |
| 2005 Sep 26 | Yes | NGC 6802, Be 52, NGC 7245, King 9 |
| 2005 Sep 27 | No | Be 52 |
| 2005 May 28 | No | Be 56 |
| 2006 Sep 18 | No | NGC 7142 |
| 2006 Sep 19 | No | Be 44 |
| 2006 Oct 19 | No | Be 56 Be 19 |
| 2007 Sep 12 | No | Be 56 |
| 2007 Sep 13 | Yes | Be 44, King 25, Be 52, Be 56 |
| 2007 Sep 14 | Yes | Be 44, King 25, NGC 6802, NGC 7245, King 9 |
| 2007 Sep 15 | Yes | Be 44, King 25, Be 52, Be 56, NGC 7245, King 9, NGC 7142 |
| 2007 Sep 16 | No | NGC 7245, King 9 |
| 2007 Oct 24 | No | Be 44 |
| 2007 Oct 25 | No | Be 56 |
| 2007 Oct 26 | Yes | NGC 6802, Be 52 |
| 2007 Oct 30 | No | Be 19 |
| 2008 May 14 | Yes | Be 44 |
| 2008 May 17 | Yes | Be 44, King 25, NGC 6802, NGC 6827, Be 52, Be 56 |
| 2008 Jul 8 | Yes | Be 44, King 25, NGC 6827, Be 56, NGC 7245, King 9 |
| 2008 Sep 27 | No | Be 56 |
| 2008 Sep 28 | No | Be 56 |
| 2008 Sep 29 | No | NGC 6802 |
| 2008 Oct 1 | Yes | Be 52, NGC 7142, Be 19 |
| 2008 Oct 2 | Yes | NGC 7142, Be 19 |
| 2009 Mar 15 | No | Be 19 |
| 2009 Mar 17 | Yes | Be 19 |

**Table 3**
Transformations to Landolt Standards (Equation (1a))

| Date | $\alpha_{bv}$ | $C_{bv}$ | $\sigma_{bv}$ | $N_{bv}$ |
|---|---|---|---|---|
| 2005 Sep 26 | −0.0166 ± 0.0035 | 1.8115 ± 0.0040 | 0.0111 | 31 |
| 2007 Sep 13 | −0.0044 ± 0.0069 | 1.3442 ± 0.0058 | 0.0176 | 57 |
| 2007 Sep 14 | −0.0084 ± 0.0061 | 1.4628 ± 0.0076 | 0.0274 | 62 |
| 2007 Sep 15 | −0.0075 ± 0.0023 | 1.3598 ± 0.0021 | 0.0115 | 231 |
| 2007 Oct 26 | −0.0019 ± 0.0089 | 1.2828 ± 0.0103 | 0.0216 | 36 |
| 2008 May 14 | 0.0057 ± 0.0054 | 1.3339 ± 0.0059 | 0.0220 | 75 |
| 2008 May 17 | −0.0123 ± 0.0033 | 1.3689 ± 0.0036 | 0.0261 | 186 |
| 2008 Jul 8 | −0.0121 ± 0.0040 | 1.4329 ± 0.0041 | 0.0187 | 102 |
| 2008 Oct 1 | −0.0119 ± 0.0058 | 1.4512 ± 0.0044 | 0.0181 | 66 |
| 2008 Oct 2 | −0.0129 ± 0.0065 | 1.5339 ± 0.0052 | 0.0229 | 81 |
| 2009 Mar 17 | −0.0260 ± 0.0057 | 1.4472 ± 0.0071 | 0.0232 | 87 |

**Table 4**
Transformations to Landolt Standards (Equation (1b))

| Date | $\alpha_b$ | $C_b$ | $\sigma_b$ | $N_b$ |
|---|---|---|---|---|
| 2005 Sep 26 | 1.0289 ± 0.0127 | 2.1308 ± 0.0124 | 0.0194 | 22 |
| 2007 Sep 13 | 1.1007 ± 0.0081 | 1.4474 ± 0.0065 | 0.0267 | 60 |
| 2007 Sep 14 | 1.0661 ± 0.0115 | 1.6222 ± 0.0123 | 0.0339 | 59 |
| 2007 Sep 15 | 1.1006 ± 0.0026 | 1.4587 ± 0.0021 | 0.0117 | 268 |
| 2007 Oct 26 | 1.0906 ± 0.0127 | 1.3936 ± 0.0123 | 0.0260 | 22 |
| 2008 May 14 | 1.0961 ± 0.0032 | 1.4472 ± 0.0032 | 0.0201 | 82 |
| 2008 May 17 | 1.0636 ± 0.0038 | 1.4699 ± 0.0036 | 0.0259 | 172 |
| 2008 Jul 8 | 1.0760 ± 0.0066 | 1.5337 ± 0.0063 | 0.0301 | 110 |
| 2008 Oct 1 | 1.0880 ± 0.0104 | 1.5922 ± 0.0068 | 0.0335 | 66 |
| 2008 Oct 2 | 1.1015 ± 0.0069 | 1.6960 ± 0.0047 | 0.0338 | 80 |
| 2009 Mar 17 | 1.0665 ± 0.0043 | 1.5809 ± 0.0056 | 0.0216 | 90 |

We used the Landolt (1992) standard star measurements to solve for nightly coefficients for the above equations. Since we did most of our observing between air mass 1.0 and 1.5 and since most of our nights appeared photometric, we used mean extinction coefficients, $k_v = 0.13$, $k_b = 0.25$, and $k_i = 0.06$, determined from a number of nights in this same period of time. On the night of 2008 May 14, there was smoke from fires in Siberia and on 2009 March 17, the sky was slightly hazy. On both nights, we measured standards over a wide range of air mass to solve for nightly extinction coefficients. For the first night, we found $k_v = 0.208 \pm 0.010$, $k_b = 0.332 \pm 0.006$, and $k_i = 0.124 \pm 0.008$ and for the second one, we obtained $k_v = 0.166 \pm 0.009$, $k_b = 0.290 \pm 0.007$, and $k_i = 0.074 \pm 0.009$. We found no evidence for significantly different extinction coefficients on the other nights. The nightly transformation coefficients (Equations (1) and (2)) are shown in Tables 3–6 along with the standard deviations of the observed minus computed values for the standards and the number of measurements per solution.

Figure 6 shows the residuals between the standard values of each standard star and the nightly calculated magnitudes, plotted versus air mass. This figure confirms that we have corrected for atmospheric extinction, within the measurement errors. The rms errors of our standard star measurements for all 11 nights taken together are 0.024 for the $B$ filter (1042 measures), 0.021 for the $V$ filter (1030 measures), and 0.020 for the $I$ filter (1028 measures).

For each program star, we solved Equations (1a) and (1b) for $V$ and $B-V$ and Equations (2a) and (2b) for $V$ and $V-I$ by least squares using all frames on which the star was identified on a given night. We next averaged the nightly magnitudes and colors weighted inversely by the calculated nightly photometric error to get preliminary calibrated magnitudes and colors for the stars in each cluster. We incorporated the data from the nights when we had no standard star measurements (see Table 2) by finding the zero-point offset between the photometry of each image (both on the nights with standard star measures and those without) and the preliminary magnitudes. Finally, using the preliminary magnitudes as local standards, we developed final transformations of all frames on all nights onto the system of the preliminary magnitudes. Given that we observed each cluster on several nights together with standards and given the errors for the standards stated above, we consider that the photometry of each of these clusters is on the standard $B$, $V$, and $I$ photometric system, as defined by Landolt (1992), within 0.01 mag in each color.

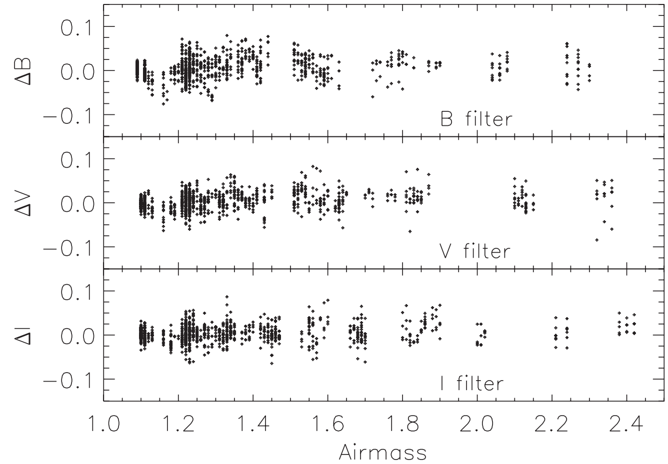


**Figure 6.** Photometric residuals of the transformations to the standard Landolt (1992) $B$, $V$, and $I$ system, plotted vs. air mass.

**Table 5**
Transformations to Landolt Standards (Equation (2a))

| Date | $\alpha_{vi}$ | $C_{vi}$ | $\sigma_{vi}$ | $N_{vi}$ |
|---|---|---|---|---|
| 2005 Sep 26 | −0.0135 ± 0.0032 | 1.8104 ± 0.0042 | 0.0109 | 31 |
| 2007 Sep 13 | −0.0044 ± 0.0067 | 1.3446 ± 0.0061 | 0.0176 | 57 |
| 2007 Sep 14 | −0.0053 ± 0.0056 | 1.4603 ± 0.0080 | 0.0274 | 62 |
| 2007 Sep 15 | −0.0074 ± 0.0021 | 1.3608 ± 0.0022 | 0.0114 | 231 |
| 2007 Oct 26 | 0.0033 ± 0.0077 | 1.2768 ± 0.0102 | 0.0214 | 36 |
| 2008 May 14 | 0.0064 ± 0.0052 | 1.3329 ± 0.0059 | 0.0219 | 75 |
| 2008 May 17 | −0.0073 ± 0.0030 | 1.3652 ± 0.0036 | 0.0265 | 186 |
| 2008 Jul 8 | −0.0094 ± 0.0036 | 1.4315 ± 0.0042 | 0.0186 | 102 |
| 2008 Oct 1 | −0.0118 ± 0.0051 | 1.4525 ± 0.0044 | 0.0179 | 66 |
| 2008 Oct 2 | −0.0147 ± 0.0060 | 1.5364 ± 0.0053 | 0.0223 | 81 |
| 2009 Mar 17 | −0.0240 ± 0.0057 | 1.4479 ± 0.0073 | 0.0234 | 87 |

**Table 6**
Transformations to Landolt Standards (Equation (2b))

| Date | $\alpha_i$ | $C_i$ | $\sigma_i$ | $N_i$ |
|---|---|---|---|---|
| 2005 Sep 26 | −0.9691 ± 0.0078 | 2.0716 ± 0.0100 | 0.0183 | 27 |
| 2007 Sep 13 | −0.9600 ± 0.0051 | 1.7164 ± 0.0049 | 0.0184 | 75 |
| 2007 Sep 14 | −0.9566 ± 0.0082 | 1.7640 ± 0.0106 | 0.0267 | 49 |
| 2007 Sep 15 | −0.9804 ± 0.0017 | 1.7571 ± 0.0019 | 0.0117 | 245 |
| 2007 Oct 26 | −0.9796 ± 0.0049 | 1.6944 ± 0.0070 | 0.0170 | 33 |
| 2008 May 14 | −0.9577 ± 0.0049 | 1.6967 ± 0.0058 | 0.0202 | 75 |
| 2008 May 17 | −0.9704 ± 0.0033 | 1.7299 ± 0.0042 | 0.0271 | 174 |
| 2008 Jul 8 | −0.9775 ± 0.0032 | 1.7860 ± 0.0037 | 0.0147 | 103 |
| 2008 Oct 1 | −0.9690 ± 0.0043 | 1.7719 ± 0.0039 | 0.0162 | 62 |
| 2008 Oct 2 | −0.9768 ± 0.0040 | 1.8296 ± 0.0038 | 0.0159 | 81 |
| 2009 Mar 17 | −0.9612 ± 0.0058 | 1.7991 ± 0.0071 | 0.0255 | 99 |

**Table 7**
Mean Photometric Errors by Cluster ($V < 18$)

| Cluster | $\langle\sigma_V\rangle$ | $n_V$ | $\langle\sigma_{B-V}\rangle$ | $n_{B-V}$ | $\langle\sigma_{V-I}\rangle$ | $n_{V-I}$ |
|---|---|---|---|---|---|---|
| Berkeley 19 | 0.003 | 466 | 0.005 | 453 | 0.004 | 461 |
| Berkeley 44 | 0.003 | 631 | 0.005 | 627 | 0.004 | 628 |
| King 25 | 0.003 | 428 | 0.008 | 425 | 0.004 | 425 |
| NGC 6802 | 0.003 | 1483 | 0.007 | 1426 | 0.005 | 1465 |
| NGC 6827 | 0.005 | 1565 | 0.009 | 1533 | 0.008 | 1554 |
| Berkeley 52 | 0.004 | 289 | 0.008 | 278 | 0.006 | 283 |
| Berkeley 56 | 0.002 | 851 | 0.004 | 831 | 0.004 | 837 |
| NGC 7142 | 0.003 | 747 | 0.004 | 698 | 0.004 | 694 |
| NGC 7245/King 9 | 0.003 | 1726 | 0.008 | 1703 | 0.004 | 1673 |

**Table 8**
Mean Photometric Errors by Magnitude

| Magnitude | $\langle\sigma_V\rangle$ | $n_V$ | $\langle\sigma_{B-V}\rangle$ | $n_{B-V}$ | $\langle\sigma_{V-I}\rangle$ | $n_{V-I}$ |
|---|---|---|---|---|---|---|
| < 14.0 | 0.003 | 239 | 0.004 | 234 | 0.005 | 227 |
| 14–15 | 0.003 | 422 | 0.004 | 416 | 0.004 | 420 |
| 15–16 | 0.002 | 1054 | 0.004 | 1039 | 0.004 | 1032 |
| 16–17 | 0.003 | 2225 | 0.005 | 2162 | 0.005 | 2184 |
| 17–18 | 0.004 | 4246 | 0.008 | 4123 | 0.006 | 4157 |
| 18–19 | 0.006 | 7535 | 0.013 | 7074 | 0.008 | 7417 |
| 19–20 | 0.009 | 13232 | 0.022 | 8784 | 0.013 | 13072 |
| > 20.0 | 0.025 | 39269 | 0.028 | 5382 | 0.031 | 39139 |

In our final photometric catalog, we included only stars observed on four or more frames in each color, with calculated standard deviations smaller than 0.1 mag. While this procedure should yield the best possible color–magnitude diagrams (CMDs), our data are incomplete at the fainter magnitudes and probably are not suitable for estimating cluster luminosity functions. Table 7 shows the mean values of the standard deviations of stars in each cluster brighter than magnitude $V = 18$. The typical errors for the brighter stars are better than 1% with only small differences from cluster to cluster. The average stellar errors for stars in all clusters taken together are tabulated as a function of magnitude in Table 8.

Table 9 presents the first few lines of a catalog of the transformed photometry for all of the clusters listed in Table 1. The remainder of the data are available in the online version of the paper. The errors listed in the table are statistical errors, derived from the dispersion in the photometry on the individual images. Possible systematic errors are not reflected in the values in the table.

## 3. A STRATEGY FOR FINDING A DISTANT CLUSTER IN A DENSE STAR FIELD

Before we can find the distances, compositions and ages of star clusters that are projected against dense stellar backgrounds, we need to develop procedures for isolating a reasonable sample of likely cluster members, and in some cases verifying that there really is a cluster there at all. Our procedure for extracting information about a cluster consists of the following steps:

After assuming a preliminary center position for the cluster, we extracted stars along strips in the $X$ and $Y$ (R.A. and decl.) directions approximately equal to the apparent visual diameter of the cluster. We then computed the marginal distributions along the $X$ and $Y$ strips and fitted Gaussian plus quadratic background functions to both marginal distributions. Figures 7 and 8 illustrate the technique for Be 19, a moderately rich cluster with good contrast from the field, and King 25, a rather poorly

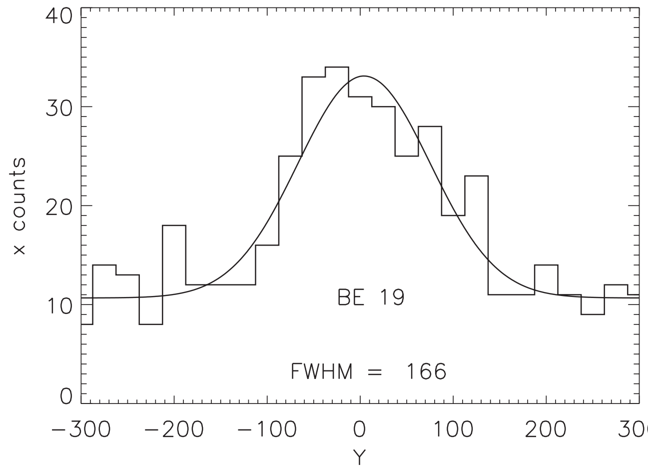


**Figure 7.** Marginal $Y$-axis distribution of stars in the field of Berkeley 19. The histogram shows the count of stars in bins 150 arcsec wide in the $X$ direction (R.A.) by 24 arcsec in the $Y$ direction. The curve shows a Gaussian fit to the distribution.

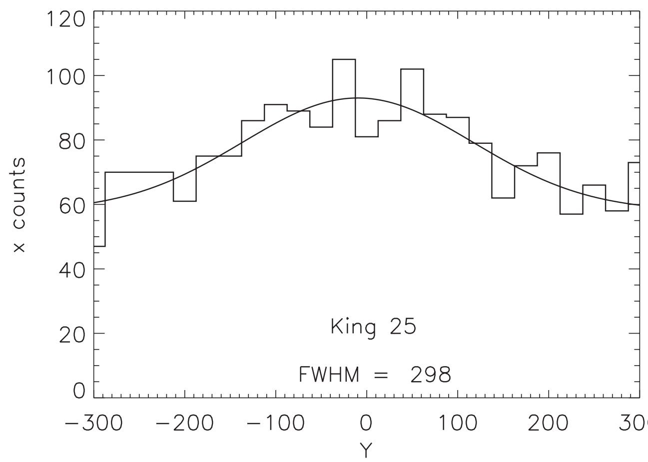


**Figure 8.** Marginal $Y$-axis distribution of stars in the field of King 25. The histogram shows the count of stars in bins 250 arcsec wide in the $X$ direction (R.A.) by 24 arcsec in the $Y$ direction. The curve shows a Gaussian fit to the distribution.

defined one. The figures show the $Y$-axis distribution only. For some of the clusters, we counted stars in a restricted range of magnitudes to maximize the contrast with the field stars. For Berkeley 44, we considered stars in the range between $V = 16$ and $V = 19$, for NGC 6802 we counted stars between $V = 14$ and $V = 17.5$, for NGC 6827, we included stars brighter than $V = 19$ and for NGC 7245 we restricted the count to stars brighter than $V = 18$.

We chose this simple, yet effective, approach to finding the cluster centers rather than fitting a more elaborate function to the full two-dimensional distribution of stars. A full two-dimensional fitting would require finer bin sizes in the star counts (with correspondingly larger fluctuations) and, with more parameters, would have fewer constraints on the derived positions.

The marginal distributions yielded improved estimates both for the cluster angular sizes and their positions, some of which are clearly off by several arcminutes in the cluster catalogs. Our positions, as determined by Gaussian fits to the marginal distributions, are good to an accuracy of better than 30 arcsec. As a measure of the cluster radii, we took two-third of the average of the FWHM values of the $X$ and $Y$ marginal distributions

**Table 9**
Photometric Catalog

| Cluster | Star | $X$ | $Y$ | $V$ | $B-V$ | $V-I$ | $N_B$ | $N_V$ | $N_I$ | Flag[a] |
|---|---|---|---|---|---|---|---|---|---|---|
| Be19 | 1 | −415.73 | 323.88 | 17.867 ± 0.003 | 1.295 ± 0.013 | ... ± ... | 4 | 5 | 0 | f |
| Be19 | 2 | −413.26 | 9.06 | 14.539 ± 0.004 | 0.867 ± 0.008 | ... ± ... | 5 | 5 | 0 | f |
| Be19 | 3 | −411.93 | −61.16 | 18.442 ± 0.009 | 1.198 ± 0.028 | ... ± ... | 5 | 5 | 0 | f |
| Be19 | 4 | −411.80 | −306.14 | 18.778 ± 0.004 | 0.813 ± 0.009 | ... ± ... | 5 | 5 | 0 | f |
| Be19 | 5 | −411.70 | 247.46 | 20.693 ± 0.025 | ... ± ... | 1.483 ± 0.030 | 0 | 5 | 5 | f |

**Notes.**
[a] Flag—m: possible cluster member; n: likely non-member; f: field star outside the cluster area; x: membership undetermined (NGC 7142 only).

(This table is available in its entirety in machine-readable and Virtual Observatory (VO) forms in the online journal. A portion is shown here for guidance regarding its form and content.)

(approximately equal to 1.5 times the Gaussian sigma of the distributions).

These radii, shown in Table 1, represent effective sizes of the clusters, within which the density of stars is significantly higher than in the surrounding field regions. Within these effective radii, we can expect that a substantial proportion of the stars are cluster members. While there may well be cluster stars beyond these radii, it would be impossible to identify individual cluster stars photometrically because of the heavy contamination by the stellar background.

The second step is to calculate a membership probability for each cluster star. We assumed that at each location in the CMD, the cluster stars are located only in the cluster region, but the field stars are distributed uniformly across both the cluster region and the surrounding field region.

So, at the position of a star *in color–magnitude space*, two counts can be made—the "CMD density" of stars in the cluster region and the "CMD density" of stars at the same color and magnitude in the surrounding field region. A measure of the membership probability is simply one minus the ratio of the field star density divided by the cluster star density at the position of the target star in the CMD. That is, we calculated

$$p = 1 - D_{\text{field}}/D_{\text{cluster}}. \quad (3)$$

To find the stellar density, we calculated the radius around each star (in the CMD) within which five stars are located. In calculating the "distance" of a star from a target star, we multiplied the color differences by a factor of 2.5, to match the scaling factor we used for presenting CMDs in the figures of this paper. For the field star density, we calculated the radius out to the fifth star around a spot with the same color and magnitude as the target star. Our density measures were further scaled by the ratio of the angular size of the cluster divided by the angular size of the field region on our detector.

For this method to work, it is necessary to cover a substantial angular field of view around the cluster to create a good statistical sample of field stars. It is also necessary to assume a uniform stellar distribution across the region. Our images cover a 13.3 arcmin field; the angular sizes of all of the clusters in our program except for NGC 7142 are sufficiently small that we could obtain a good field star sample with a single pointing at the position of the cluster. Fortunately, the contrast between the cluster and the surrounding field population is larger in the NGC 7142 region than in the other cluster fields.

For each of the other clusters, we used the estimated cluster radius given in Table 1 to define the cluster region and we defined a field region consisting of stars beyond an outer radius $\sqrt{2}$ times the cluster radius. We did not include stars in a buffer region between the cluster radius and the field radius in our analysis. The buffer region stars (which may include both cluster stars and field stars) are included in Table 9 labeled as field stars. There is a tradeoff between choosing a small radius for the field region to maximize the likelihood that the field region is representative of the field star population within the cluster radius, and choosing a larger radius that will be mostly free of actual cluster members. There still could be some cluster stars in our field regions, but our goal was to achieve the maximum visibility of the cluster sequences, not to derive a complete census of cluster stars.

In Figures 9–18, we present $[V, (B - V)]$ and $[V, (V - I)]$ CMDs for each cluster. The left-hand diagram in each figure consists of all stars within the field of our detector. The middle diagram includes stars between $\sqrt{2}$ and $\sqrt{3}$ times the cluster radius, i.e., a ring within the field region of area equal to the cluster area. We assume all stars in the middle diagram are field stars. The right-hand diagram includes stars within the cluster radius that also have a photometric membership probability of greater than 50%, as defined by Equation (3).

## 4. A PROCEDURE FOR QUANTITATIVE CLUSTER ANALYSIS

Since metallicity, reddening, and temperature of a star all affect the broadband color indices similarly, it is not ordinarily possible to fit a theoretical stellar isochrone unambiguously to a cluster main sequence, unless the reddening and composition of the cluster are known independently. This important point is often ignored.

The common practice of "fitting" theoretical isochrones to CMDs is often done simply by visual comparison of the cluster and the isochrone, but an isochrone is simply a line showing the possible colors and magnitudes for theoretical models of a particular age. The actual probability of finding a star varies widely along the isochrone, so at some places along the isochrone there will hardly ever be actual stars and at others, there will be many. Thus, an isochrone simply does not look enough like an actual cluster CMD.

Furthermore, even after applying our extraction procedure, the field star contamination of distant clusters can be substantial. In some cases, only two features of the cluster CMD are distinguishable: the upper main sequence and turnoff regions and the red giant "clump," the location of disk population core-helium-burning stars.

The red giant clump represents a stationary phase as a disk star evolves through the CMD, so in most clusters older than a few hundred million years, there is a noticeable concentration of stars with similar temperatures and luminosities. Over a wide range of compositions and ages, red giant clump stars occupy a

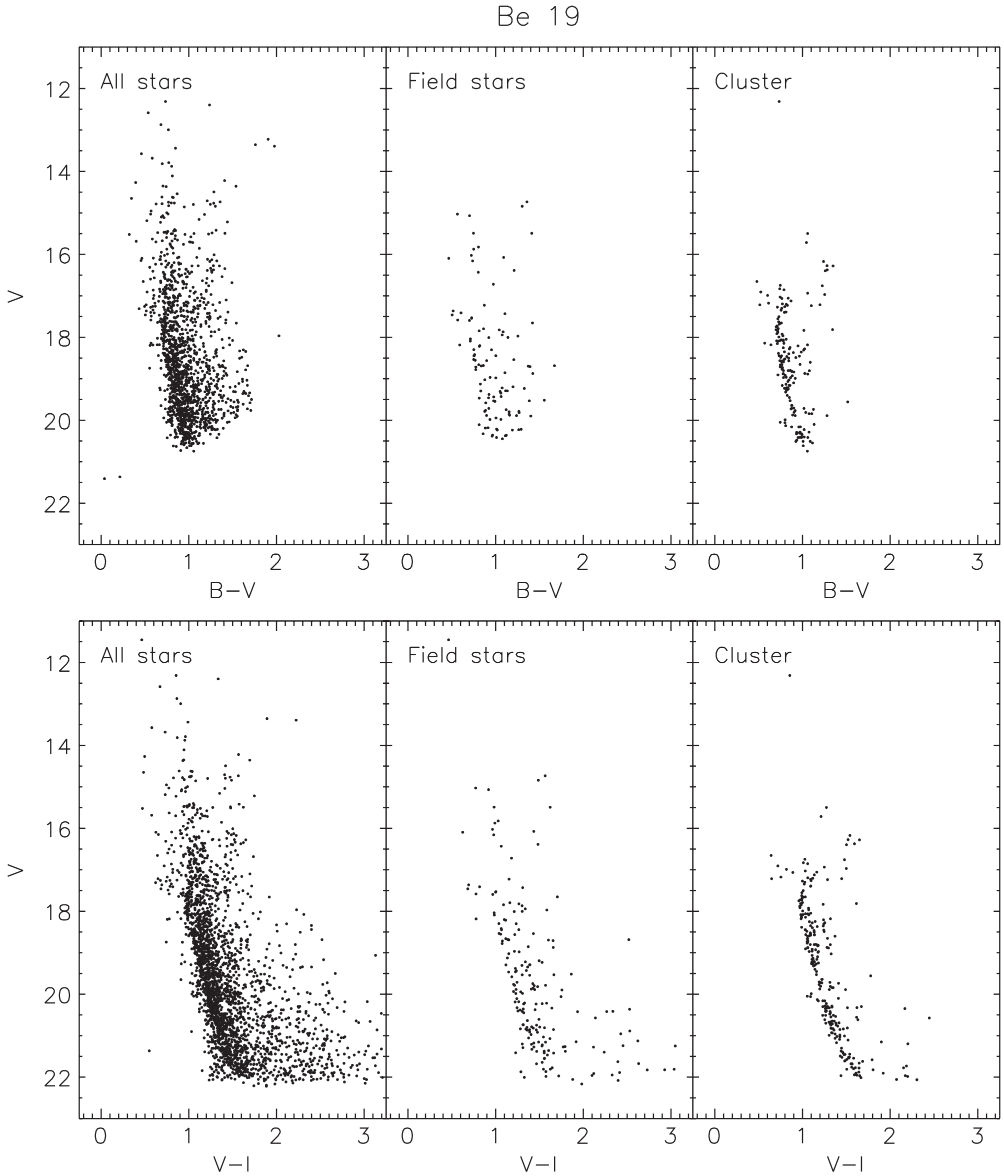


**Figure 9.** Berkeley 19 CMD. Top: [$V$, $(B - V)$] photometry for all stars in the detector field of view (left), stars in an outer field ring equal in area to the cluster region (center), and photometrically determined cluster members (right). Bottom: the same for [$V$, $(V - I)$] photometry.

relatively small range of color and absolute magnitude, making the clump stars potential standard candles. Although the name is rather prosaic, the topic has been much discussed (see, e.g., Sarajedini 1999; Grocholski & Sarajedini 2002; Pietrzyński et al. 2003; Van Helschoecht & Groenewegen 2007).

As a cluster ages from about the age of the Hyades to the age of the oldest clusters in the Galactic disk, the turnoff becomes fainter and redder, whereas the clump does not change much. Janes & Phelps (1994) created a "morphological age index," or "MAI," by comparing the differences in luminosity and color between the main-sequence turnoff and the red giant branch. Salaris et al. (2004) used main-sequence fitting to a selection of clusters to develop a calibration for a slightly modified MAI index and used this calibration to derive the ages of 71 old clusters.

Several more sophisticated approaches have been taken to estimate properties of star clusters in the presence of field stars and binary star members of the cluster. For the nearest clusters, detailed analyses can be made of the clusters, including, for example, using the cluster white dwarf population as a constraint on cluster properties (e.g., De Gennaro et al. 2009). For more distant clusters, more indirect methods of finding cluster parameters are usually required. One of the more successful methods is the synthetic CMD method of Aparicio et al. (1990) and Tosi et al. (1991) (see also Bragaglia & Tosi 2006; Bragaglia et al. 2009). They created synthetic CMDs starting from the original stellar evolutionary tracks from which isochrones are derived. They populated a CMD according to the probability that a star will actually be found at a particular location, assuming some initial mass function. They also added in some binary stars and a field star population characteristic of the particular direction. This approach makes it possible to compare their synthetic diagrams directly with that of actual clusters, or other stellar populations.

Girardi & Salaris (2001) (see also Salaris & Girardi 2002) also referred directly to the Padova models to find the mean $M_V$ and $M_I$ values of stars in the core-helium-burning phase of evolution.

We took a somewhat similar approach, but we started instead from the published Padova isochrones (Girardi et al. 2000;

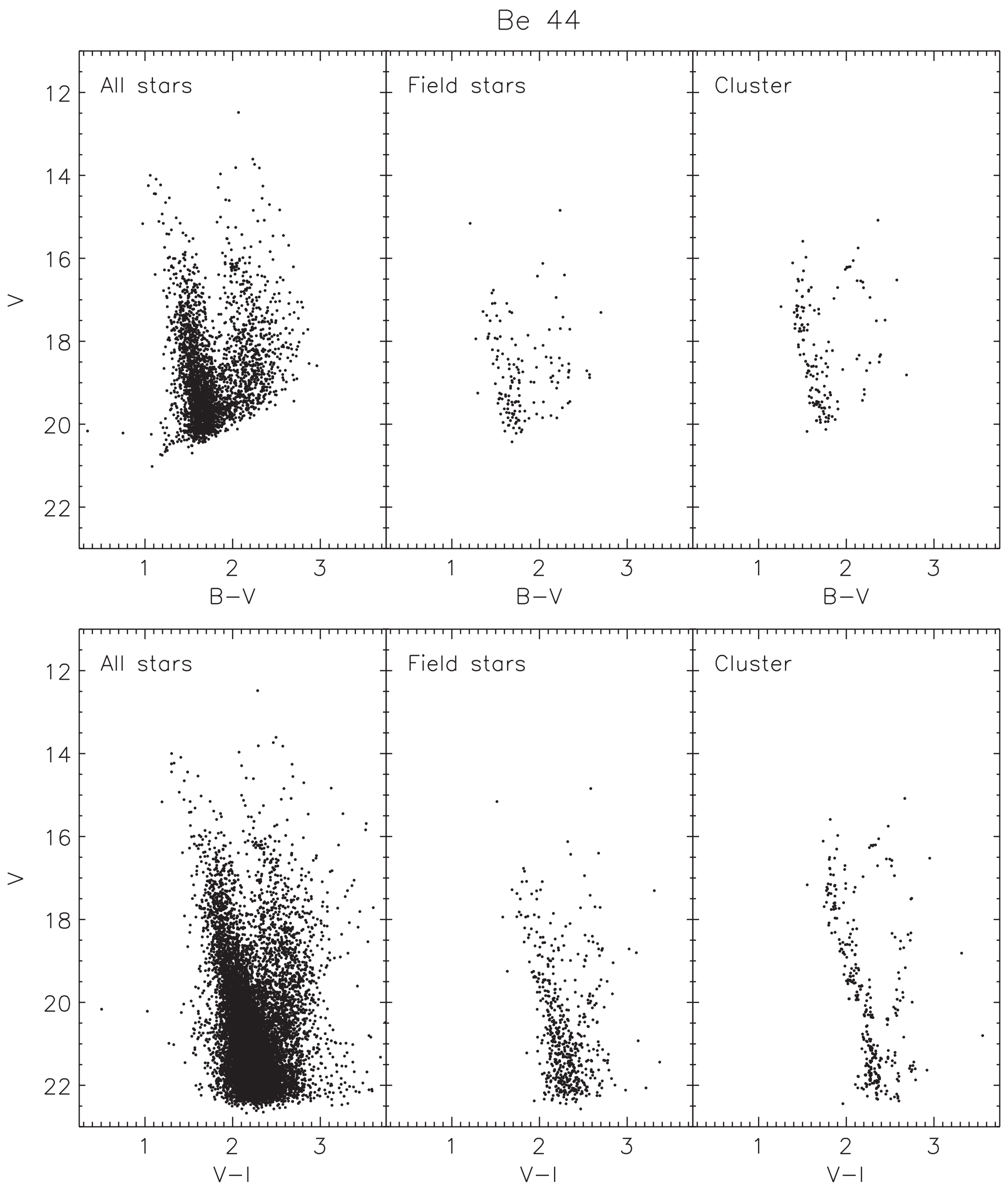


**Figure 10.** Berkeley 44 CMD. Top: $[V, (B - V)]$ photometry for all stars in the detector field of view (left), stars in an outer field ring equal in area to the cluster region (center), and photometrically determined cluster members (right). Bottom: the same for $[V, (V - I)]$ photometry.

Marigo et al. 2008). The Padova isochrones (available online at http://pleiadi.pd.astro.it) are tabulated as a function of the model mass. As shown by Gallart et al. (2005), the Padova models produce isochrones consistent with a number of other models near the main-sequence turnoff.

We selected isochrones with a range of ages and compositions, and used a Monte Carlo approach to populate synthetic CMDs by choosing random masses within the mass range of a particular isochrone. In effect, we assumed a constant mass function, where the number of stars per unit mass interval is independent of mass; although this may not be the "correct" present-day mass function, it is an adequate assumption for our purposes. We then added in assumed photometric errors (we chose a value of 0.02 in magnitude and color), to make a visually more realistic diagram. An example of this is shown in Figure 19, which shows a synthetic CMD of a cluster with 10,000 stars. The synthetic CMDs can be analyzed in the same way as the observed clusters.

To find the color of the red giant clump (either the theoretical one or the observed one), we started with an initial visual estimate of the clump position. At the estimated $V$ magnitude of the clump, we slid a box of size 0.75 mag high in $V$ by 0.15 mag wide in color index through the CMD, stepping by 0.075 mag in color at a time. At each position of the box, we calculated the mean value of the color index. We took the mean value of the color index in the box with the largest number of stars as a starting estimate for the next iteration; this process converges in 2–3 iterations.

We used a similar procedure to find the color of the main-sequence turnoff, which we define as the bluest point on the CMD. To find the turnoff, we passed a window 0.5 magnitude tall in $V$ and 0.1 mag wide in color index across the CMD, stepping by 0.25 in $V$ magnitude and 0.05 in color. At each $V$ position, we recorded the median value of the color index at the location with the largest number of stars. We took as the turnoff, the bluest of these median values.

The results of this analysis of the synthetic diagrams are given in Tables 10 and 11, for solar composition isochrones ($X = 0.019$) and metal-poor isochrones ($X = 0.008$), corresponding approximately to $[\mathrm{Fe/H}] = -0.38$.

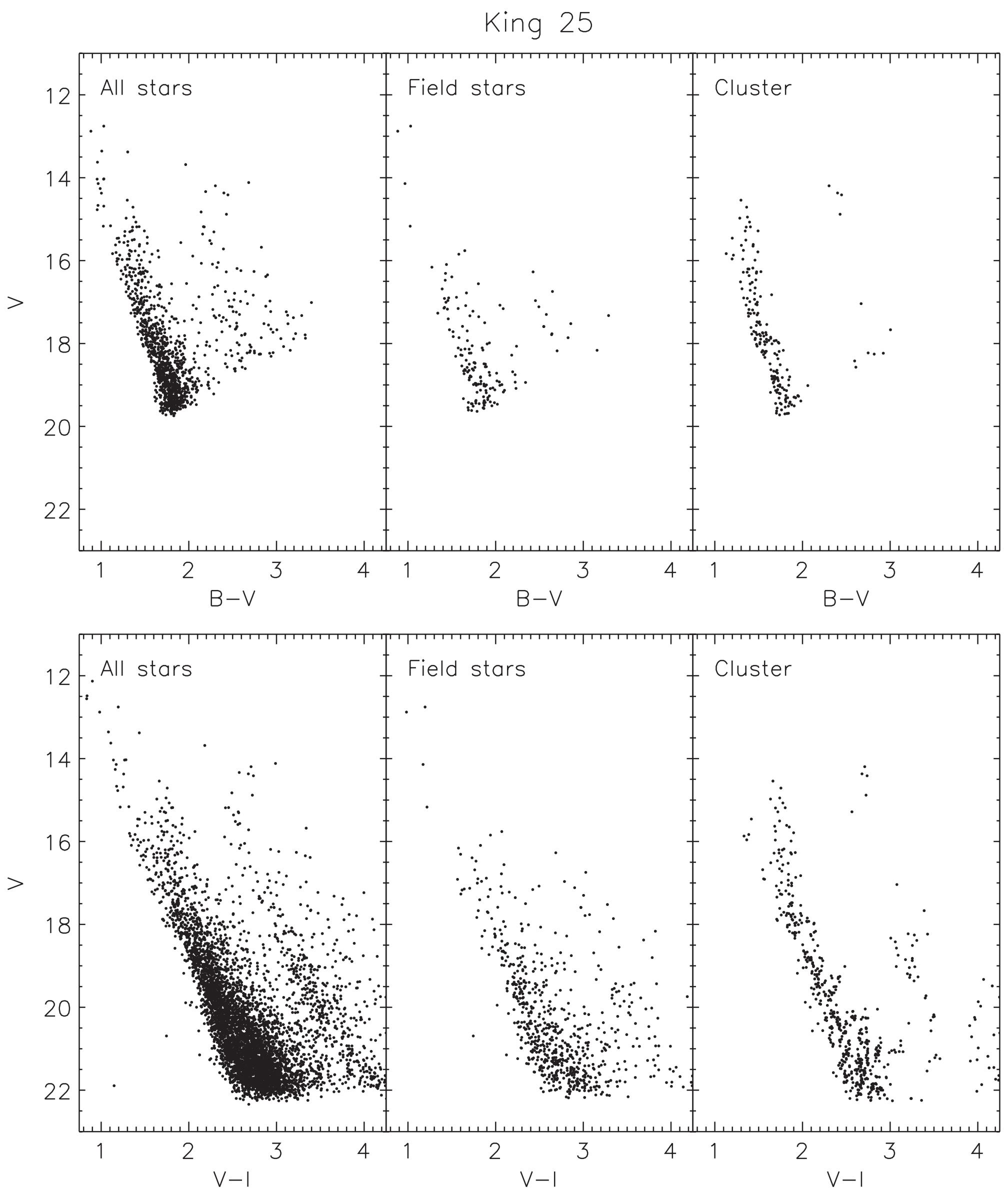


**Figure 11.** King 25 CMD. Top: $[V, (B-V)]$ photometry for all stars in the detector field of view (left), stars in an outer field ring equal in area to the cluster region (center), and photometrically determined cluster members (right). Bottom: the same for $[V, (V-I)]$ photometry.

We used the same method to calculate the turnoff and clump colors for the clusters. The clusters add two additional complicating factors—the presence of binaries in the cluster sequences and the contamination by the background field stars. Fortunately, near the turnoff, binaries will have nearly the same colors as single stars, so the their effect on the measured turnoff will be small. Except for NGC 7245 which lacks a clump, the cluster sequences are defined well enough to permit reasonable estimates of the clump and turnoff. These values are given in Table 12.

Finally, by interpolating the values for the clusters from Table 12 in Tables 10 and 11, we obtained estimates for the cluster reddenings, distances, and ages. We were able to make four measures of the reddening and age—two using the $B-V$ and $V-I$ colors to interpolate in Table 10, assuming solar composition, and two more by interpolating in Table 11, assuming a metal-poor composition. For each cluster, we made an initial estimate of the reddening taking the intrinsic $(B-V)$ or $(V-I)$ color of the clump to be 1.05 (solar composition) or 0.90 (the metal-poor case). With the initial reddening estimate, we found the color of the turnoff, and using the appropriate composition table, we made an initial age estimate. Then, once we had an age estimate, we derived a revised value of the clump color to recalculate the reddening and a final value for the age. With the final values for the reddening and age, we used Tables 10 and 11 once more to get the absolute magnitude of the clump and the distance modulus.

In calculating the reddening, we used the ratio $E(V-I)/E(B-V)$ given by Dean et al. (1978),

$$\frac{E(V-I)}{E(B-V)} = 1.25[1+0.06(B-V)_{\rm o}+0.014(E(B-V)]. \quad (4)$$

We also assumed a total-to-selective absorption ratio, $A_V = 3.1E(B-V)$.

The results of this analysis are shown in Table 13.

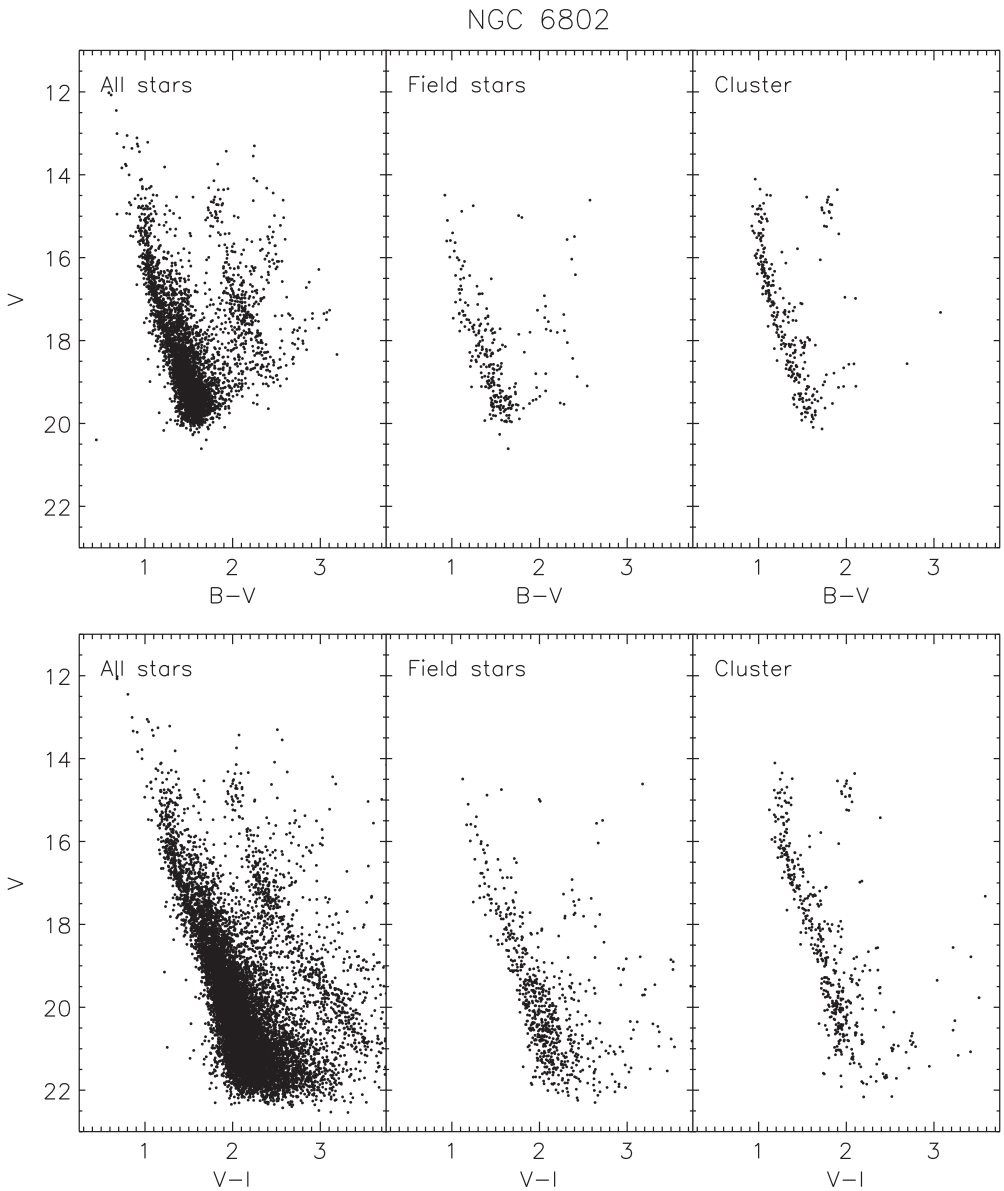


**Figure 12.** NGC 6802 CMD. Top: $[V, (B-V)]$ photometry for all stars in the detector field of view (left), stars in an outer field ring equal in area to the cluster region (center), and photometrically determined cluster members (right). Bottom: the same for $[V, (V-I)]$ photometry.

## 5. ERROR DISCUSSION

One major advantage of the procedure, we have followed in this paper over conventional main-sequence fitting, is that we can do a step-by-step analysis of the uncertainties.

1. *Photometric errors*. The random photometric errors for the brighter stars, from which we derived the cluster parameters, are generally less than $\pm 0.01$ mag (see Tables 7 and 8). We have also estimated that the zero-point errors in the photometric standardization (see Section 3) are less than $\pm 0.01$ mag. Since the fiducial points tabulated in Table 12 are the combined result of several stars, we can safely conclude that the actual photometric errors do not contribute more than about 0.01 mag to the final result.
2. *Clump and turnoff positions*. Neither the clump nor the turnoff represents single points in the CMD. Although both are at relatively well-defined locations, the detailed distribution of stars within the CMD depends on the accidental distribution of masses along the cluster sequences and on the choice of the window size we used. To study the stability of our method, we created repeated synthetic CMDs of 100 or 250 stars for a selection of ages. We then compared the calculated clump and turnoff colors with the appropriate values in Tables 10 and 11 (which are derived from 10,000 star synthetic CMDs), to get a typical error for the clump or turnoff position. We found that at all ages, the rms variation in color, resulting from the random positions of stars along the isochrone, was rather uniformly a little under $\pm 0.02$, and the rms $V$ magnitude variation was about $\pm 0.08$ mag. These values represent the inherent "jitter" in the position of the clump and turnoff resulting from the random positions of stars in the CMD.

   To these uncertainties, which are present in both the synthetic CMDs and the observed clusters, we need to add about $\pm 0.01$ mag of possible systematic error in the observed colors and magnitudes, as discussed above, plus an additional amount resulting from the inclusion of field stars and cluster binary stars near the main-sequence

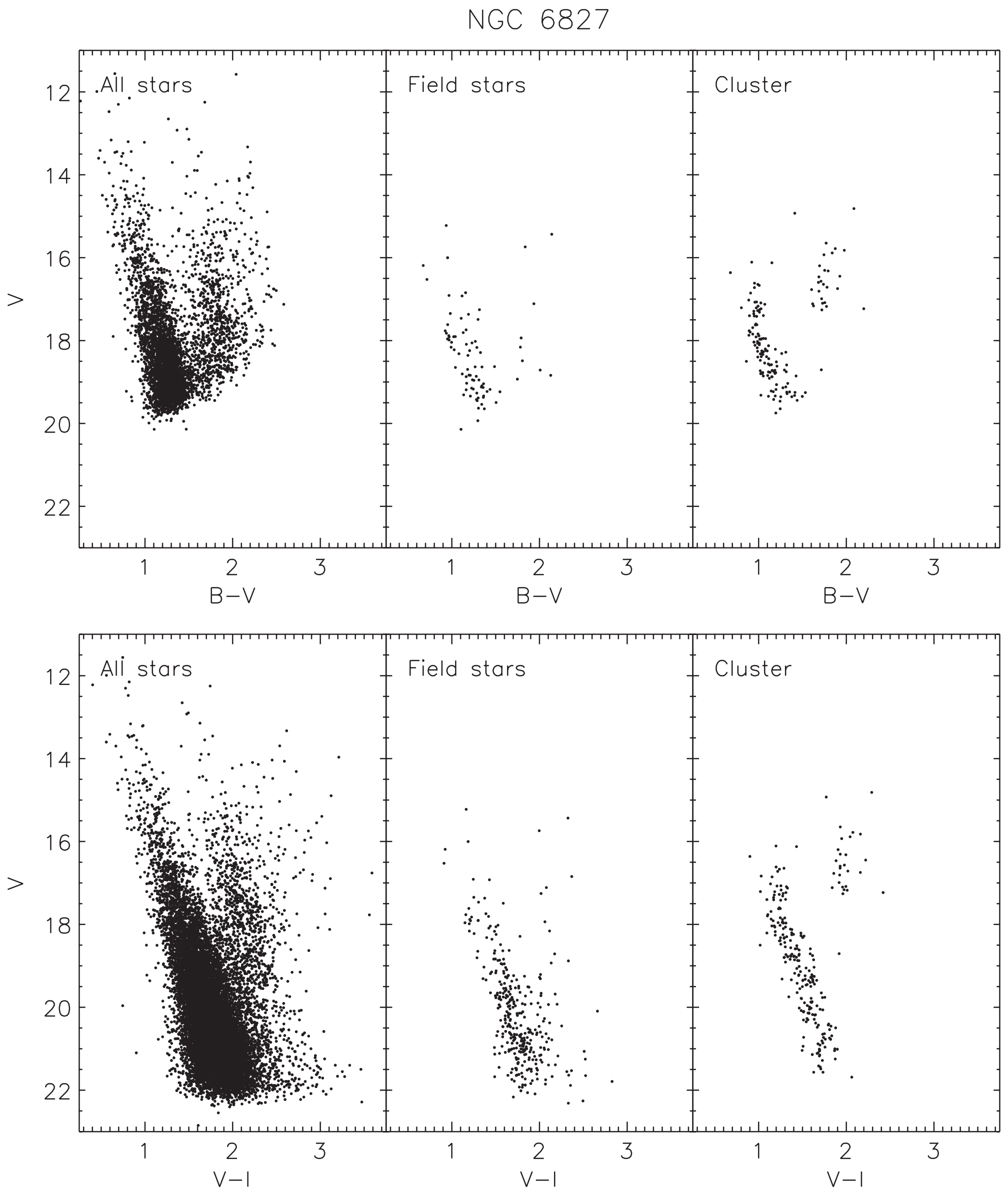


**Figure 13.** NGC 6827 CMD. Top: $[V, (B - V)]$ photometry for all stars in the detector field of view (left), stars in an outer field ring equal in area to the cluster region (center), and photometrically determined cluster members (right). Bottom: the same for $[V, (V - I)]$ photometry.

turnoff. If there are several such stars randomly placed within the window, they can be expected to add another $\pm0.02$ mag error in color index and $\pm0.05$ mag in $V$. We estimate then that the combined effects of these error sources will be about $\pm0.04$ mag in color index and $\pm0.10$ mag in $V$.

3. *Composition*. The most uncertain parameter in this process is the cluster composition. Since most disk stars, including the open clusters, have metallicities between about solar and one-half solar, we have assumed that the main-sequence turnoff and clump colors will typically lie between the values in Tables 10 and 11. At a fixed age, the colors of the metal-poor isochrones are approximately 0.12 mag bluer than the solar composition isochrones. So, if the average is used, the uncertainty in the colors resulting from the unknown composition will be on the order of $\pm0.06$ mag.
4. *Reddening*. Since the color of the clump is virtually constant with age, the error in the calculated reddening is a combination of the uncertainty in the clump position and the unknown value of the composition. These are largely independent of each other, so the typical reddening uncertainty is the quadrature sum of the composition error and the clump location error, or about $\pm0.07$ mag. If there is no observable clump in a cluster CMD (e.g., NGC 7245), then this method fails and some other way has to be found to derive the cluster parameters.
5. *Age*. The error in log(age) is primarily derived from the reddening uncertainty (which in turn depends on the composition uncertainty). A change in the reddening of $\pm0.07$ mag results in a typical log(age) change of about $\pm0.15$, with the values in Tables 10 and 11.
6. *Distance modulus*. The calculated distance modulus depends on the value of the absolute magnitude of the clump, corrected for absorption. Since the clump luminosity is only a slow function of age for stars older than about $10^9$ years, the reddening and composition errors are the dominant error

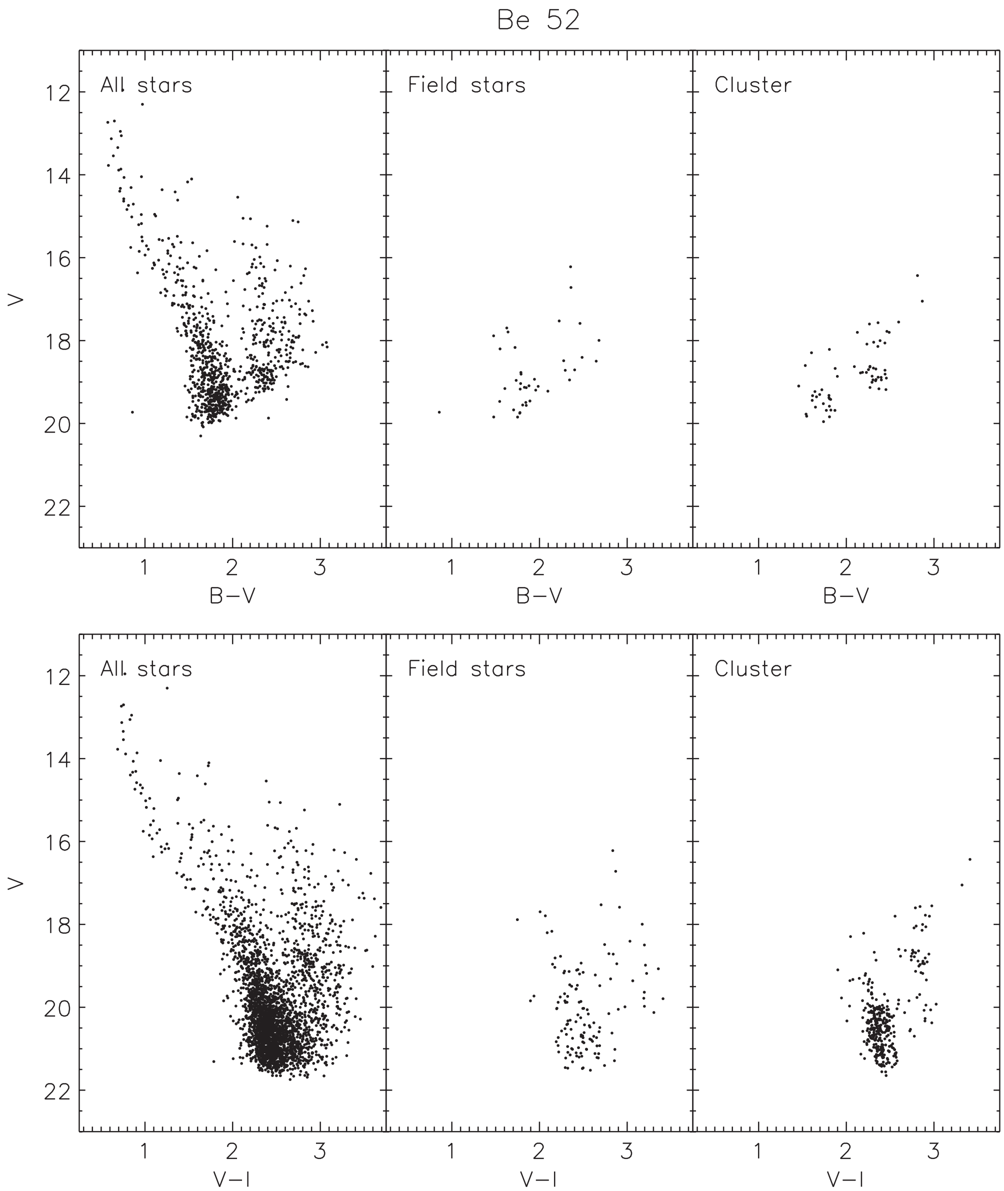


**Figure 14.** Berkeley 52 CMD. Top: $[V, (B-V)]$ photometry for all stars in the detector field of view (left), stars in an outer field ring equal in area to the cluster region (center), and photometrically determined cluster members (right). Bottom: the same for $[V, (V-I)]$ photometry.

sources. Tables 10 and 11show that at fixed age, the metal-poor isochrones are about 0.25 mag brighter and 0.12 mag bluer than the solar isochrones. So, for a given clump apparent magnitude, the metallicity effects on reddening and clump luminosity partially cancel each other, and the combined effects of absorption and composition plus the "jitter" in the clump position lead to an uncertainty in the distance modulus of about ±0.25.

The calculated standard deviations based on the four measurements of the reddening and log(age) and the two measurements of the distance modulus are given in Table 12. Although the errors listed in the table are somewhat smaller than the estimates discussed above, they are based on the assumption of completely independent measurements, and do not reflect all the uncertainties. For that reason, we estimate that the total uncertainties are approximately the same as the numbers provided above, $E(B-V) = \pm 0.07$, log(age) $= \pm 0.15$, and $(m-M)_\circ = \pm 0.25$.

## 6. NOTES ON THE INDIVIDUAL CLUSTERS

### *6.1. Berkeley 19*

This cluster was observed photographically by Christian (1980), who was able to reach just to the main-sequence turnoff. Her preliminary results indicated an age about 3 Gyr and a distance modulus about 13.5. Using new CCD photometry, Hasagawa et al. (2008) found an age of 1.8 Gyr, a reddening, $E(V-I) = 0.60$ and a distance modulus of 14.29. Neither study reached a limiting magnitude much below the main-sequence turnoff, so these estimates are very preliminary. Our photometry (Figure 9) shows a clearly defined main sequence reaching to magnitude 22 in $[V, (V-I)]$ and magnitude 21 in $[V, (B-V)]$. Only a few possible red clump stars appear in the CMDs, but the application of the analytical procedure described above leads to results consistent with the previous studies. Although the statistical errors listed in Table 12 are rather small, the actual uncertainty is much larger, dominated in this case by the small

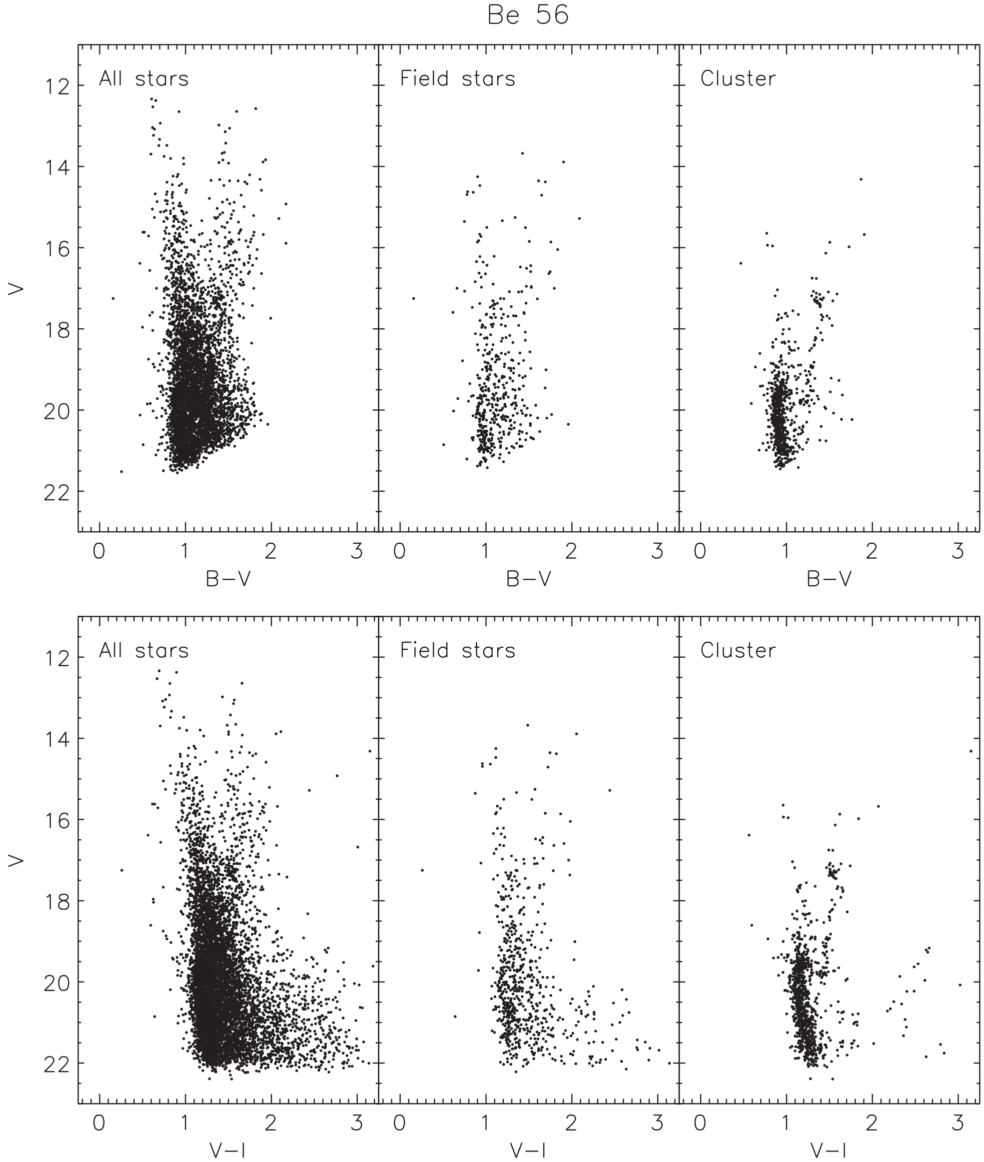


**Figure 15.** Berkeley 56 CMD. Top: $[V, (B - V)]$ photometry for all stars in the detector field of view (left), stars in an outer field ring equal in area to the cluster region (center), and photometrically determined cluster members (right). Bottom: the same for $[V, (V - I)]$ photometry.

number of clump stars. Because of its sparseness, little else can be said about the cluster, without identifying more red giants (perhaps with the help of proper motions or radial velocities) or with deep, multicolor photometry.

### 6.2. Berkeley 44

The Be 44 region is an extremely dense field; in our 13.3 arcmin field of view, we catalogued over 10,000 stars brighter than magnitude 22. Nevertheless, our marginal distribution for this cluster (Figure 7), limited to stars brighter than magnitude 19, shows a well-defined peak. Our CMD for Be 44 is shown in Figure 10. In spite of the dense background field, the cluster parameters are reasonably well determined.

Using a version of the cluster extraction method described here, Carraro et al. (2006) isolated likely cluster members and concluded that the photometry was consistent with a cluster about 1.3 Gyr in age, reddened by $E(B - V) = 1.40$ mag at a distance modulus of $V - M_V = 15.60$. However, there is a substantial color offset in the Carraro et al. photometry relative to the present photometry. The location of the red giant clump

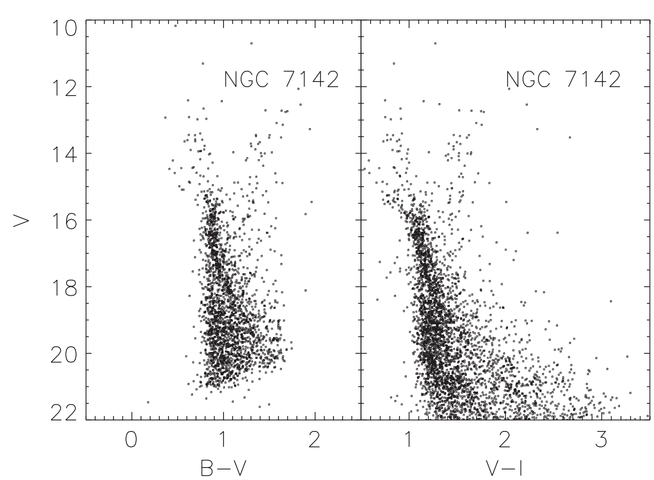


**Figure 16.** NGC 7142 $[V, (B - V)]$ (left diagram) and $[V, (V - I)]$ (right diagram) CMDs of the entire 13.3 arcmin field. Because the cluster diameter is about 8 arcmin, there are not enough stars in the surrounding field for a good field star sample.

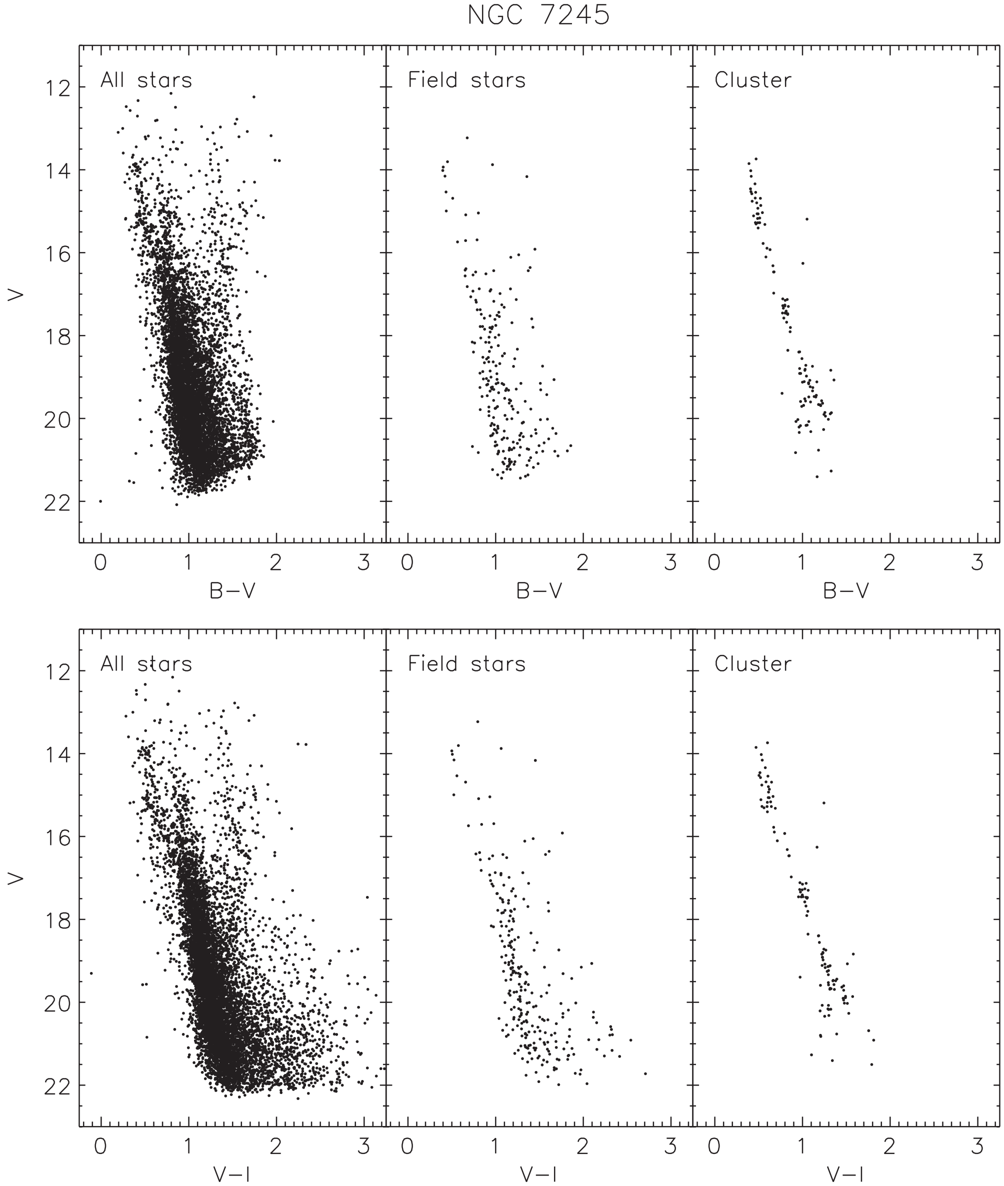


**Figure 17.** NGC 7245 CMD. Top: $[V, (B-V)]$ photometry for all stars in the detector field of view (left), stars in an outer field ring equal in area to the cluster region (center), and photometrically determined cluster members (right). Bottom: the same for $[V, (V-I)]$ photometry.

is shifted by approximately 0.2 mag to larger values in both magnitude and color (both $B-V$ and $V-I$) relative to this paper.

### 6.3. King 25

The marginal distributions through the center of this cluster (Figure 8) show only a slight enhancement of stellar density near the center of the field. Although the "cluster" appears to have a moderately well-defined main sequence and possibly a few clump stars, these are not clearly separated from the field distribution. Our analysis of this cluster has somewhat larger errors than most of the other clusters, and there may not be an actual cluster, or it is at best a sparsely populated group of heavily reddened stars. Carraro et al. (2005) reached the same conclusion.

### 6.4. NGC 6802

Figure 2 shows that this cluster is rather more prominent than some of the others, although it is still embedded in an extremely rich star field. The marginal distributions indicate a radius about 100 arcsec.

Previous photometric studies of the cluster include Hoag et al. (1961) and Sirbaugh et al. (1995). In the latter study (published as an abstract only), Sirbaugh et al. found an age for the cluster of 1 Gyr, a reddening, $E(B-V) = 0.94$, and a true distance modulus, $(m-M)_\circ = 10.78$, reasonably close to our values.

### 6.5. NGC 6827

Although it is projected against an extremely rich star field, NGC 6827 is quite distinctly visible (see Figure 3). Our marginal distributions support this observation when we restrict the sample to stars brighter than magnitude 19. We find a cluster radius of 75 arcsec, but although the cluster is visually distinct, the extracted cluster CMD (Figure 13) is rather indistinct, possibly because of the richness of the background field and the large reddening.

As they did for Be 44, Carraro et al. (2006) derived values for the turnoff and clump luminosities and colors that are about

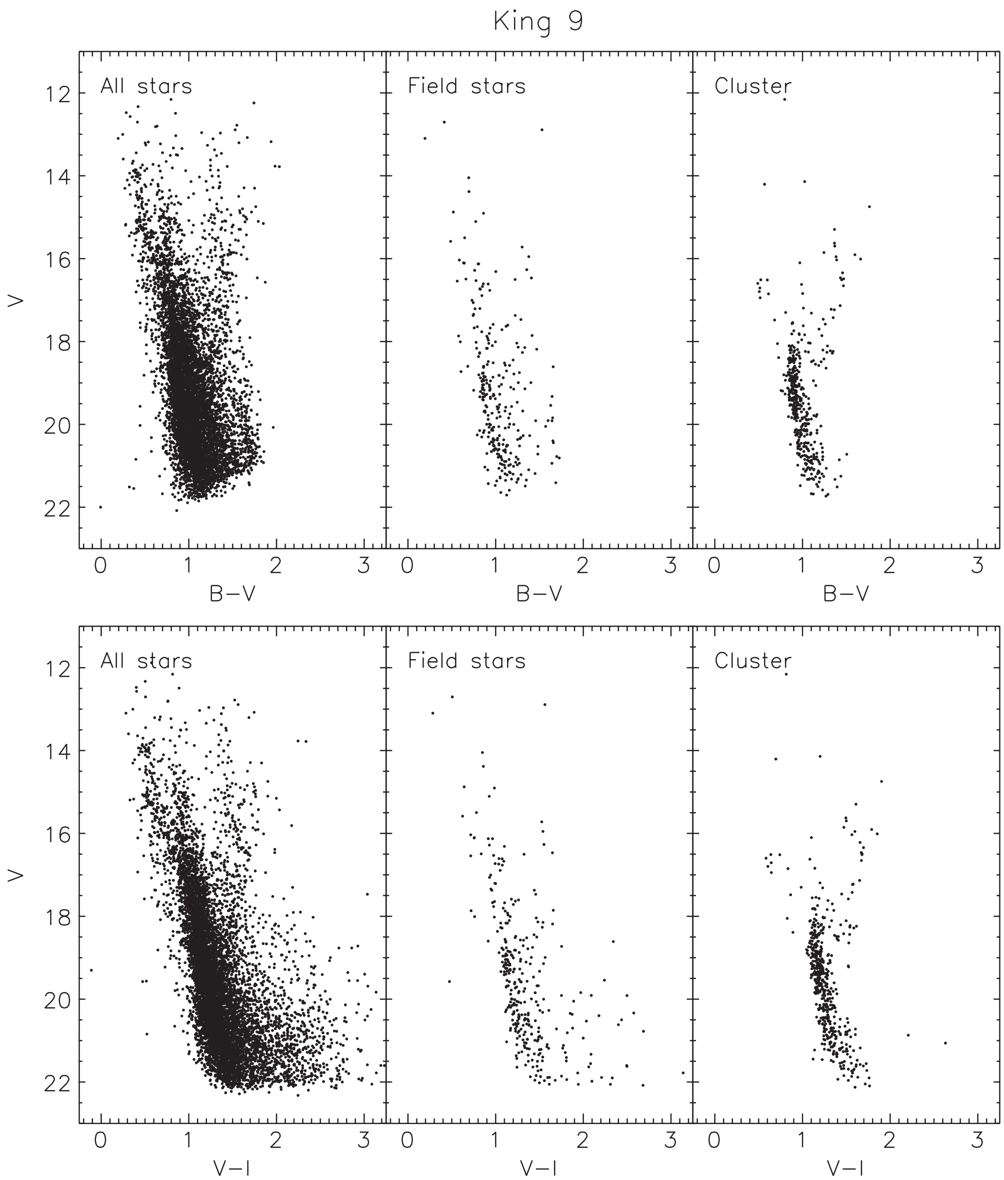


**Figure 18.** King 9 CMD. Top: $[V, (B-V)]$ photometry for all stars in the detector field of view (left), stars in an outer field ring equal in area to the cluster region (center), and photometrically determined cluster members (right). Bottom: the same for $[V, (V-I)]$ photometry. The NGC 7245 main sequence is visible in the field diagrams (see Figure 17).

0.2 mag larger than we have found. Consequently, they derived a somewhat larger reddening, $E(B-V) = 1.05$, and smaller distance modulus, $(m-M)_\circ = 13.06$.

### 6.6. Berkeley 52

Berkeley 52 is extremely faint and obviously rather reddened. Nevertheless, Figure 14 clearly shows a rich, moderately old cluster. It is the faintest of the clusters in this sample, with a somewhat broadened main sequence, possibly the result of differential reddening across the cluster. For this cluster as well, the Carraro et al. (2006) colors are shifted with respect to the present photometry. They found $E(B-V) = 1.50$ and $(m-M)_\circ = 13.45$ for Be 52.

### 6.7. Berkeley 56

This is a rather well-defined cluster in a somewhat less crowded field than most of the others. Our analysis shows that although the reddening is more moderate than most of the others, it is the most distant cluster of the group. Carraro et al. (2006) also found a large distance but moderate reddening: $E(B-V) = 0.40$ and $(m-M)_\circ = 15.41$. These are close to the present values, although there is still an offset in the photometry.

### 6.8. NGC 7142

Because NGC 7142 covers a larger angular diameter than the other clusters, it was not possible to do a membership analysis in the same way as the others. The apparent angular diameter of the cluster is about 8 arcmin, judging from visual inspection of the cluster region.

There have been several photographic and photoelectric studies of the cluster (see van den Bergh & Heeringa 1970). More recently, Crinklaw & Talbert (1991) studied NGC 7142 and found a distance modulus of 11.4, and an age between that of M67 and NGC 188, consistent with our value of 6.9 Gyr. They also concluded that the reddening across the cluster is variable,

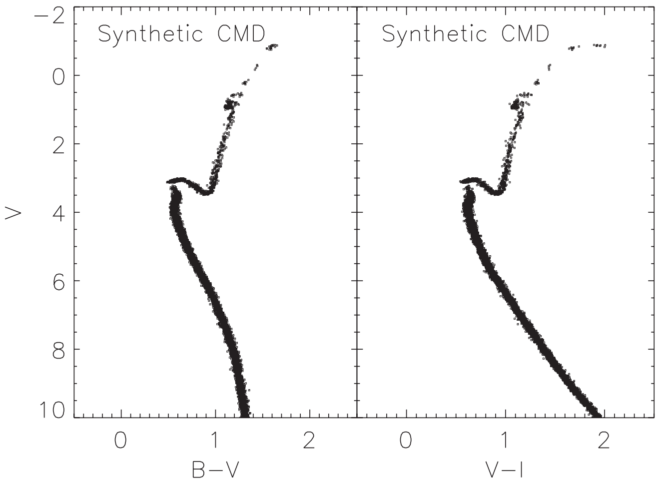


**Figure 19.** Synthetic CMD derived from a log(age) = 9.3, solar composition ($X = 0.019$) Padova isochrone (Marigo et al. 2008). The CMD contains 10,000 stars with randomly chosen masses in the mass range of the published isochrone. Gaussian errors with $\sigma = 0.02$ mag have been added. We used synthetic CMDs like this to derive the calibrations of Tables 10 and 11.

**Table 10**
Padova Solar Composition Isochrones—Turnoff and Clump Colors and Clump Luminosity

| Age | $(B-V)_{\rm to}$ | $(V-I)_{\rm to}$ | $(M_V)_{\rm cl}$ | $(B-V)_{\rm cl}$ | $(V-I)_{\rm cl}$ |
|---|---|---|---|---|---|
| 8.500 | −0.038 | −0.040 | −0.532 | 1.027 | 0.982 |
| 8.600 | 0.002 | 0.001 | −0.156 | 1.010 | 0.972 |
| 8.700 | 0.056 | 0.049 | 0.147 | 1.005 | 0.971 |
| 8.800 | 0.121 | 0.123 | 0.511 | 0.998 | 0.968 |
| 8.900 | 0.198 | 0.210 | 0.728 | 0.999 | 0.972 |
| 9.000 | 0.272 | 0.306 | 0.926 | 1.004 | 0.978 |
| 9.100 | 0.337 | 0.394 | 1.003 | 1.017 | 0.989 |
| 9.150 | 0.369 | 0.429 | 0.886 | 1.035 | 1.006 |
| 9.200 | 0.393 | 0.461 | 0.800 | 1.070 | 1.033 |
| 9.250 | 0.418 | 0.487 | 0.796 | 1.085 | 1.045 |
| 9.300 | 0.445 | 0.514 | 0.796 | 1.101 | 1.059 |
| 9.400 | 0.490 | 0.555 | 0.829 | 1.118 | 1.083 |
| 9.500 | 0.535 | 0.595 | 0.873 | 1.135 | 1.098 |
| 9.600 | 0.569 | 0.622 | 0.933 | 1.146 | 1.113 |
| 9.700 | 0.581 | 0.637 | 0.960 | 1.153 | 1.118 |
| 9.750 | 0.595 | 0.651 | 0.960 | 1.161 | 1.116 |
| 9.800 | 0.612 | 0.664 | 0.997 | 1.162 | 1.119 |
| 9.850 | 0.628 | 0.677 | 1.010 | 1.155 | 1.114 |
| 9.900 | 0.649 | 0.695 | 1.013 | 1.159 | 1.122 |
| 9.950 | 0.666 | 0.706 | 1.070 | 1.163 | 1.110 |
| 10.000 | 0.688 | 0.724 | 1.094 | 1.176 | 1.134 |

which could explain the relatively poorly defined CMDs of Figure 16.

### 6.9. NGC 7245

Located in the SW corner of the field of view of King 9 (see Figure 4) is another cluster, NGC 7245. Because there are no clump stars evident in the CMD it is not possible to apply the same analysis we applied to the other clusters. We find log(age) = 8.65, based on the turnoff colors, assuming the reddening is the same as King 9 [$E(B-V) = 0.45$]. This is essentially identical to the age we found for King 25, so after adjusting for the difference in reddening we get a distance modulus of approximately $(m-M)_\circ = 12.7$. That is to say, for this one cluster, we relied on the traditional method of "fitting" the NGC 7245 CMD to that of King 25. Subramaniam & Bhatt (2007) also observed this cluster, finding $E(B-V) = 0.45$, $(m-M)_{\rm o} = 12.9 \pm 0.2$, and an age of 400 Myr. Because NGC 7245 is much younger and much closer to us than King 9, it is unlikely that there is any connection between the two clusters.

**Table 11**
Padova $Z = 0.008$ Isochrones—Turnoff and Clump Colors and Clump Luminosity

| Age | $(B-V)_{\rm to}$ | $(V-I)_{\rm to}$ | $(M_V)_{\rm cl}$ | $(B-V)_{\rm cl}$ | $(V-I)_{\rm cl}$ |
|---|---|---|---|---|---|
| 8.500 | −0.067 | −0.065 | −1.077 | 0.792 | 0.833 |
| 8.600 | −0.042 | −0.043 | −0.573 | 0.826 | 0.861 |
| 8.700 | −0.010 | −0.013 | 0.000 | 0.827 | 0.864 |
| 8.800 | 0.036 | 0.028 | 0.341 | 0.839 | 0.871 |
| 8.900 | 0.089 | 0.085 | 0.614 | 0.845 | 0.881 |
| 9.000 | 0.151 | 0.160 | 0.803 | 0.858 | 0.889 |
| 9.100 | 0.217 | 0.251 | 0.770 | 0.878 | 0.903 |
| 9.150 | 0.245 | 0.294 | 0.529 | 0.914 | 0.931 |
| 9.200 | 0.280 | 0.343 | 0.523 | 0.931 | 0.945 |
| 9.250 | 0.310 | 0.387 | 0.527 | 0.945 | 0.957 |
| 9.300 | 0.338 | 0.423 | 0.536 | 0.956 | 0.971 |
| 9.400 | 0.382 | 0.480 | 0.606 | 0.973 | 0.980 |
| 9.500 | 0.422 | 0.521 | 0.650 | 0.980 | 0.989 |
| 9.600 | 0.436 | 0.536 | 0.716 | 0.994 | 1.000 |
| 9.700 | 0.465 | 0.567 | 0.766 | 0.993 | 1.000 |
| 9.750 | 0.484 | 0.587 | 0.774 | 0.997 | 0.993 |
| 9.800 | 0.503 | 0.603 | 0.805 | 1.004 | 1.001 |
| 9.850 | 0.521 | 0.618 | 0.778 | 0.990 | 0.994 |
| 9.900 | 0.535 | 0.631 | 0.773 | 0.982 | 0.983 |
| 9.950 | 0.547 | 0.642 | 0.882 | 1.001 | 0.997 |
| 10.000 | 0.563 | 0.655 | 0.760 | 0.987 | 0.989 |

**Table 12**
Turnoff and Clump Colors and Clump Magnitude for Program Clusters

| Cluster | $(B-V)_{\rm to}$ | $(V-I)_{\rm to}$ | $(M_V)_{\rm cl}$ | $(B-V)_{\rm cl}$ | $(V-I)_{\rm cl}$ |
|---|---|---|---|---|---|
| Berkeley 19 | 0.72 | 0.99 | 16.30 | 1.27 | 1.54 |
| Berkeley 44 | 1.44 | 1.81 | 16.20 | 2.03 | 2.31 |
| King 25 | 1.40 | 1.84 | 14.32 | 2.39 | 2.70 |
| NGC 6802 | 1.01 | 1.29 | 14.69 | 1.80 | 1.93 |
| NGC 6827 | 0.98 | 1.21 | 16.54 | 1.72 | 1.92 |
| Berkeley 52 | 1.80 | 2.26 | 18.84 | 2.30 | 2.79 |
| Berkeley 56 | 0.89 | 1.14 | 17.32 | 1.37 | 1.53 |
| King 9 | 0.89 | 1.14 | 16.45 | 1.44 | 1.68 |
| NGC 7245 | 0.48 | 0.60 | ... | ... | ... |
| NGC 7142 | 0.87 | 1.09 | 13.76 | 1.36 | 1.50 |

**Table 13**
Results for the Target Clusters

| Cluster | $E(B-V)$ (mag) | log(age) | $(m-M)_\circ$ (mag) | $R_{\rm GC}$ (kpc) |
|---|---|---|---|---|
| Berkeley 19 | 0.32 ± 0.06 | 9.40 ± 0.08 | 14.48 ± 0.02 | 16.4 |
| Berkeley 44 | 0.98 ± 0.04 | 9.46 ± 0.08 | 12.48 ± 0.07 | 7.1 |
| King 25 | 1.52 ± 0.09 | 8.67 ± 0.07 | 10.37 ± 0.31 | 7.8 |
| NGC 6802 | 0.84 ± 0.05 | 8.98 ± 0.07 | 11.25 ± 0.03 | 7.4 |
| NGC 6827 | 0.78 ± 0.03 | 8.98 ± 0.01 | 13.29 ± 0.06 | 7.2 |
| Berkeley 52 | 1.28 ± 0.05 | 9.55 ± 0.13 | 14.06 ± 0.06 | 8.5 |
| Berkeley 56 | 0.36 ± 0.06 | 9.78 ± 0.13 | 15.22 ± 0.22 | 13.5 |
| NGC 7142 | 0.32 ± 0.05 | 9.84 ± 0.05 | 11.85 ± 0.05 | 9.4 |
| NGC 7245 | (0.45) | (8.65) | (12.7) | 9.5 |
| King 9 | 0.45 ± 0.05 | 9.42 ± 0.08 | 14.33 ± 0.05 | 12.2 |

### 6.10. King 9

This cluster is well defined (see Figure 4) and like Berkeley 56 is relatively less reddened than some of the others. Subramaniam

& Bhatt (2007) found a reddening of $0.37 \pm 0.04$ to the cluster, or using a metal-poor isochrone, they found $E(B - V) = 0.47$. With the lower reddening (assuming solar abundance), they found $(m - M)_0 = 14.5 \pm 0.3$ and an age of 3.0 Gyr. These values are in reasonable agreement with our results.

## 7. DISCUSSION

In spite of the fact that most of the clusters listed in this sample are heavily reddened and in crowded fields, we have been able to extract moderately well-defined CMDs. Three requirements need to be met to make this a practical procedure.

1. There has to be an actual cluster at the location under study, with enough members to make a significant contrast with the background, at least within some range of magnitudes. King 25 marginally satisfies this criterion.
2. Even if there is a cluster, it may not be accessible to optical studies because of excessive interstellar reddening and extinction. King 25 is the most heavily reddened of the program clusters although it is also the nearest. IR photometry or spectroscopy would be required to further disentangle King 25. It is worth noting that fainter than about magnitude 20 or so, most of the clusters in this sample become indistinguishable from the background field. The cluster stars are simply lost in the great mass of the background stellar population.
3. In order for the method proposed here to work at all, the field surrounding the cluster must be rather uniform in population and in reddening. If there is a gradient in the field population or irregular obscuration, some more elaborate process would be necessary.

In spite of the fact that we have no information about the composition of the clusters, we have been able to derive reasonable estimates of the reddenings, distances, and ages. If two clusters had the same observed turnoff and clump colors and luminosities, but different metallicities, the more metal-poor cluster would be more heavily reddened, but somewhat younger. The metal-poor clump has a brighter absolute magnitude, but the larger reddening means that the distance modulus of the metal-poor cluster would be slightly smaller than that of the metal-rich one. So by relying on the color of the turnoff and the color and magnitude of the clump, the lack of knowledge of the metallicity has a relatively small effect on the results.

This particular group of open clusters represents a diverse sampling of the Galactic stellar population. The youngest cluster in the group, NGC 7245, is only about 450 million years old, and the oldest, NGC 7142, is about 7 Gyr in age. Berkeley 44 is approximately 7.1 kpc from the Galactic center, if the Sun is at 8.5 kpc from the Galactic center, and Berkeley 19 is 16.4 kpc from the Galactic center.

We thank the referees for comments that helped us to clarify several sections of this paper. This research has been supported by the National Science Foundation under grants AST-0440936 and AST-0507655 and by Boston University. We have also made use of the WEBDA database, operated at the Institute for Astronomy at the University of Vienna.

*Facility:* Perkins (PRISM)

## REFERENCES

Aparicio, A., Bertelli, G., Chiosi, C., & Garcia-Pelayo, J. M. 1990, A&A, 240, 262
Archinal, B., & Hynes, S. 2003, Star Clusters (Richmond, VA: Willman-Bell)
Bragaglia, A., Carretta, E., Gratton, R., & Tosi, M. 2009, in IAU Symp. 254, The Galaxy Disk in Cosmological Context, ed. J. Andersen, J. Bland-Hawthorn, & B. Nordström (Cambridge: Cambridge Univ. Press), 227
Bragaglia, A., & Tosi, M. 2006, AJ, 131, 1544
Carraro, G., Janes, K. A., & Eastman, J. D. 2005, MNRAS, 364, 179
Carraro, G., Subramanian, A., & Janes, K. A. 2006, MNRAS, 371, 1301
Christian, C. A. 1980, AJ, 85, 700
Crinklaw, G., & Talbert, F. D. 1991, PASP, 103, 536
Dean, J. F., Warren, P. R., & Cousins, A. W. J. 1978, MNRAS, 183, 569
De Gennaro, S., von Hippel, T., Jefferys, W. H., Stein, N., van Dyk, D., & Jeffery, E. 2009, ApJ, 696, 12
Dias, W. S., Alessi, B. S., Moitinho, A., & Lepine, J. R. D. 2002, A&A, 389, 871
Dias, W. S., Alessi, B. S., Moitinho, A., & Lepine, J. R. D. 2007, VizieR Online Catalog: B/ocl
Dutra, C. M., & Bica, E. 2000, A&A, 359, 347
Gallart, C., Zoccali, M., & Aparicio, A. 2005, ARA&A, 43, 387
Girardi, L., Bressan, A., Bertelli, G., & Chiosi, C. 2000, A&A, 141, 371
Girardi, L., & Salaris, M. 2001, MNRAS, 323, 109
Grocholski, A. J., & Sarajedini, A. 2002, AJ, 123, 1603
Hasagawa, T., Sakamoto, T., & Malasan, H. L. 2008, PASJ, 60, 1267
Hoag, A. A., Johnson, H. L., Iriarte, B., Mitchell, R. I., Hallam, K. L., & Sharpless, S. 1961, Publ. US Nav. Obs., 17, 347
Janes, K. A., & Heasley, J. N. 1993, PASP, 105, 527
Janes, K. A., & Phelps, R. L. 1994, AJ, 108, 1773
Landolt, A. U. 1992, AJ, 101, 340
Landolt, A. U. 2009, AJ, 137, 4186
Marigo, P., Girardi, L., Bresson, A., Groenewegen, M. A. T., Silva, L., & Granato, G. L. 2008, A&A, 482, 883
Mermilliod, J.-C., & Paunzen, E. 2003, A&A, 410, 511
Pietrzyński, G., Gieren, W., & Udalski, A. 2003, AJ, 125, 2494
Salaris, M., & Girardi, L. 2002, MNRAS, 337, 332
Salaris, M., Weiss, A., & Percival, S. M. 2004, A&A, 414, 163
Sarajedini, A. 1999, AJ, 118, 2321
Sirbaugh, R. D., Lewis, K. A., & Friel, E. D. 1995, BAAS, 27, 1439
Subramaniam, A., & Bhatt, B. C. 2007, MNRAS, 377, 829
Tosi, M., Greggio, L., Marconi, G., & Focardi, P. 1991, AJ, 102, 951
van den Bergh, S., & Heeringa, R. 1970, A&A, 9, 209
Van Helschoecht, V., & Groenewegen, M. A. T. 2007, A&A, 463, 559